

DEPARTMENT OF INFORMATICS

TECHNISCHE UNIVERSITÄT MÜNCHEN

Bachelor's Thesis in Informatics: Games Engineering

**Finite volume and discontinuous Galerkin
methods for hyperbolic partial differential
equations**

Lisa Scheller

DEPARTMENT OF INFORMATICS

TECHNISCHE UNIVERSITÄT MÜNCHEN

Bachelor's Thesis in Informatics: Games Engineering

**Finite volume and discontinuous Galerkin
methods for hyperbolic partial differential
equations**

**Finite Volumen- und diskontinuierliche
Galerkin-Verfahren für hyperbolische
partielle Differentialgleichungen**

Author:	Lisa Scheller
Supervisor:	Univ.-Prof. Dr. Michael Bader
Advisor:	MSc Leonhard Rannabauer
Submission Date:	15.12.2017

I confirm that this bachelor's thesis in informatics: games engineering is my own work and I have documented all sources and material used.

Munich, 15.12.2017

Lisa Scheller

Abstract

This bachelor's thesis gives an overview over hyperbolic partial differential equations, especially the shallow water equations. Several numerical methods for solving these kind of problems are described and compared, focusing on finite volume methods and discontinuous Galerkin methods. Since for those methods numerical flux functions are used, some of them are also explained. An analytic solution for dam break problems is developed for later error computing and convergence analysis. The implementation of both a finite volume solver, as well as a discontinuous Galerkin solver, is described in detail, also which scenarios were used and what results were computed. This is used to compare finite volume and discontinuous Galerkin approaches. After that, the error of the methods is computed and the order of convergence of the method determined. The methods are then compared in regard to this.

Zusammenfassung

Diese Bachelorarbeit gibt einen Überblick über hyperbolische partielle Differentialgleichungen, insbesondere über die Shallow Water Equations. Mehrere numerische Methoden zur Lösung von derartigen Gleichungen werden beschrieben und verglichen, mit einem besonderen Fokus auf Finite-Volumen-Methoden und diskontinuierliche Galerkin-Verfahren. Da diese Methoden numerische Flussannäherungen nutzen, werden einige davon ebenfalls erläutert. Es wird eine analytische Lösung für Dammbruch-Probleme entwickelt, um damit später den Fehler der numerischen Methoden berechnen zu können und das Konvergenzverhalten dieser Methoden untersuchen zu können. Die Implementierung sowohl eines Finite-Volumen-Lösers als auch eines Diskontinuierlichen-Galerkin-Lösers wird detailliert beschrieben. Zusätzlich wird genauer aufgeführt, welche Szenarios verwendet wurden und welche Ergebnisse berechnet wurden. Darauf aufbauend werden dann die beiden Methoden miteinander verglichen. Zuletzt wird das Fehlerverhalten sowie die Konvergenzordnung der Verfahren untersucht und erneut ein Vergleich zwischen den Methoden durchgeführt.

Nomenclature and abbreviations

List of Abbreviations

CFL condition Courant-Friedrichs-Lewy condition

DG discontinuous Galerkin

FEM finite elements method

FV finite volumes

ODE ordinary differential equation

PDE partial differential equation

Nomenclature

Δx cell size, $x_{i+1/2} - x_{i-1/2}$

$f'(q)$ Jacobi matrix of $f(q)$

q vector of unknowns

q_x partial derivative $\frac{\delta q}{\delta x}$

Contents

Abstract	iii
Zusammenfassung	iv
Nomenclature and abbreviations	v
1 Introduction	1
2 The shallow water equations	2
2.1 Hyperbolic partial differential equations	2
2.1.1 Definition	2
2.1.2 Classification	3
2.1.3 Examples	4
2.1.4 Numerical difficulties	5
2.2 The shallow water equations	5
2.2.1 Equations in one dimension	5
2.2.2 Properties	6
2.2.3 Example problems	7
2.2.4 Two-dimensional equations	7
3 Methods for solving hyperbolic partial differential equations	9
3.1 Finite Differences	9
3.1.1 General description	9
3.1.2 Advantages and disadvantages	9
3.2 Finite Volumes	10
3.2.1 General description	10
3.2.2 Advantages and disadvantages	11
3.2.3 The Courant-Friedrichs-Lewy condition	12
3.2.4 Flux approximations	12
3.3 Finite Elements	14
3.3.1 General description	14
3.3.2 Advantages and disadvantages	14

3.4	Discontinuous Galerkin methods	15
3.4.1	General description	15
3.4.2	Nodal and modal formulation	16
3.4.3	Handling more complex equations	17
3.4.4	Advantages and disadvantages	18
3.4.5	Comparison between the methods	18
3.5	Summary of numerical integration methods	19
3.5.1	Explicit Euler	19
3.5.2	Implicit Euler	20
3.5.3	Heun's method	20
3.5.4	Runge-Kutta methods	20
4	Analytic solution of the dam-break problem	22
4.1	Introduction	22
4.1.1	Shock waves	22
4.1.2	Rarefaction waves	23
4.2	Different types of wave composition	23
4.2.1	Two shocks	23
4.2.2	Two rarefaction waves	24
4.2.3	One rarefaction wave and one shock	25
4.3	Solving the problem	26
4.3.1	Determining the boundaries of each section	26
4.3.2	Getting the middle state	26
4.3.3	Computing the shock speed	27
4.3.4	Determining the behaviour inside a rarefaction wave	27
4.3.5	Putting the solution together	28
5	Implementation	29
5.1	Computed scenarios	29
5.1.1	Continuous initial conditions - Gaussian distribution	29
5.1.2	Discontinuous initial conditions - dam-break problem	31
5.1.3	Exact solution of the used dam-break problem	32
5.2	Details of implementation	32
5.2.1	General information	32
5.2.2	Switches to use finite volume methods	33
5.2.3	Switches to use discontinuous Galerkin methods	33
5.2.4	Other switches	34
5.3	Used methods	34
5.3.1	Finite Volumes	34

Contents

5.3.2	Discontinuous Galerkin	37
5.4	Comparison of finite volume and discontinuous Galerkin	40
5.4.1	Advection equation	40
5.4.2	Shallow Water Equations	42
5.5	Error estimation	44
5.5.1	Advection equation	44
5.5.2	Shallow water equations	44
6	Conclusion	52
	Appendix	A
1	Detailed derivation of matrices for discontinuous Galerkin method . . .	A
2	Overview over computed errors	B
2.1	Advection equation - finite volumes	B
2.2	Advection equation - discontinuous Galerkin	B
2.3	Advection equation - discontinuous Galerkin and midpoint method	B
2.4	Shallow water equations - finite volumes	C
2.5	Shallow water equations - discontinuous Galerkin	C
2.6	Shallow water equations - discontinuous Galerkin and midpoint method	D
	List of Figures	E
	List of Tables	G
	Bibliography	H

1 Introduction

This thesis gives an overview over the usage of finite volume methods and discontinuous Galerkin methods for solving hyperbolic partial differential equations, especially for the one-dimensional shallow water equations with discontinuous initial conditions, the so called dam break problem. The shallow water equations are an important member of hyperbolic partial differential equations (PDEs) and have to be numerically solved in a lot of hydrodynamic problems. Also, while there are known analytic solutions for many one dimensional initial conditions, which simplifies the error computing process, most higher-dimensional problems don't have a known analytic solution. Since numerical solutions to a one-dimensional dam-break problem have to be able to handle the resulting setup of shock waves and rarefaction waves, this scenario tests the ability of the used method to deal with the main obstacles that present when trying to solve a hyperbolic PDE numerically. This makes these initial conditions good test cases to determine the suitability of a method to solve hyperbolic PDEs. This knowledge can then be used for the approximation of more difficult PDEs with no known analytic solutions or solving higher-dimensional problems.

First an overview over hyperbolic PDEs and especially the shallow water equations is given. Since the solving of Riemann problems is vital to solve a dam break problem, this concept will be explained. The next chapter includes an overview over several numerical methods to solve hyperbolic PDEs and list their advantages and disadvantages. Finite volume and discontinuous Galerkin methods will be covered in more detail. Also, some numerical flux functions will be introduced. They are later used in the implementation. For discontinuous Galerkin methods, the difference between the nodal and modal form will be explained. The implementation uses only a nodal approach. A short overview over some numerical integration methods is given. The remaining part of the chapter is used to explain how a dam break problem can be solved analytically. The following chapter contains the details of the implementation of the finite volume and discontinuous Galerkin solver, which scenarios were used, what results were obtained for finite volumes as well as discontinuous Galerkin methods and how the methods compare to each other. Finally the error computing methods will be described and the error analyzed and compared to the theoretically expected error.

2 The shallow water equations

2.1 Hyperbolic partial differential equations

2.1.1 Definition

Partial differential equations (PDEs) are used to describe a multitude of problems. In contrast to ordinary differential equations (ODEs), PDEs contain partial derivatives, whereas ODEs only contain derivatives of one variable. There are a multitude of phenomenons that can be described by PDEs, ranging from fluid mechanics and traffic simulation over thermodynamic problems to quantum mechanics. In this bachelor's thesis I restrict myself to a certain subclass of PDEs, the so-called hyperbolic PDEs. The core equations of this thesis, the shallow water equations, which will be introduced in detail in the next section, as well as the standard advection equation, are hyperbolic PDEs.

Definition 2.1.1. "A linear system of the form

$$q_t + Aq_x = 0$$

is called hyperbolic if the $m \times m$ matrix A is diagonalizable with real eigenvalues."[Lev04, p. 31]

This is a one-dimensional, homogenous, first-order system of PDEs. q is a vector from \mathbb{R}^m that contains the unknowns of the equations and A is a $m \times m$ matrix. The restriction that the matrix has to be diagonalizable means that it must be possible to describe A in the following way:

$$A = S \cdot D \cdot S^{-1} \tag{2.1}$$

where D is a diagonal matrix, and S is a basis transformation onto the basis defined by all eigenvectors of A .

Other types of PDEs are elliptic or parabolic PDEs.

2.1.2 Classification

There are several sub-groups of hyperbolic PDEs, in regard to the eigenvalues of A as well as in regard to the structure of the equations.

Eigenvalues

Since a symmetric matrix is always diagonalizable with real eigenvalues, all symmetric matrices can be used to describe a hyperbolic problem [Lev04, p.32]. These equations are called symmetric hyperbolic.

If the matrix has distinct eigenvalues and is diagonalizable, the system of PDEs is called strictly hyperbolic [Lev04, p.32].

In contrast, a matrix that is not diagonalizable but has real eigenvalues is called weakly hyperbolic [Lev04, p.32].

Structure of equations

In the simplest case of a hyperbolic PDE, A is not a matrix, but a constant scalar. Equation (2.1.1) simplifies to

$$q_t + a q_x = 0 \quad (2.2)$$

and a has to be real for the system to be hyperbolic.

If the scalar a or the matrix A are time-dependent or depend on another value (e.g. $a(x, t)$, $A(x, p)$), they have to fulfill the criteria for a system of hyperbolic PDEs for each value of t (or in the examples also for x and p) [Lev04, p.33].

Conservation laws A special group of hyperbolic PDEs are called conservation laws. In the simplest case (one dimension) they have the following structure:

$$q(x, t)_t + f(q(x, t))_x = 0 \quad (2.3)$$

or in the quasilinear form [Lev04, p.17]

$$q_t + f'(q) q_x = 0 \quad (2.4)$$

$f(q)$ can be linear as well as non-linear in regard to q .

The integral formulation This formulation can also be used to describe a conservation law, in fact it is the more fundamental form to describe one, because it also holds across discontinuities.

The integral formulation of a hyperbolic conservation law looks as follows:

$$\frac{d}{dt} \int_{x_1}^{x_2} q(x, t) dx = F(x_2, t) - F(x_1, t) \quad (2.5)$$

$f(x, t)$ represent fluxes going either into or out from the element. The differential formulation ((2.3)), which is used mostly, can be derived from the integral formulation under the assumption that q is smooth. [Lev04, p.16]

Weak solutions However, to be able to treat naturally occurring discontinuities, we need to extend the native definition of a solution by the weak formulation. This leads (detailed description [Lev04, p.215]) to the following equation:

$$\int_0^\infty \int_{-\infty}^\infty [q\phi_t + f(q)\phi_x] dx dt = - \int_0^\infty q(x, 0)\phi(x, 0) dx \quad (2.6)$$

Definition 2.1.2. "The function $q(x, t)$ is a weak solution of the conservation law $q_t + f(q)_x = 0$ with given initial data $q(x, 0)$ if (2.6) holds for all functions ϕ in C_0^1 ." [Lev04, p.215]

Here C_0^1 describes all functions with compact support (the function has non-zero values inside a compact subset of the domain and zero for all points outside this subset) that are continuously differentiable.

2.1.3 Examples

Only very few hyperbolic PDEs are easy to solve. Their complexity ranges from one-dimensional, linear equations to multidimensional nonlinear PDEs. For most of these problems, especially if they are nonlinear or multidimensional, no analytic solution is known. One example of a very basic hyperbolic PDE is the one-dimensional advection equation with constant speed:

$$q_t + uq_x = 0 \quad (2.7)$$

where u is the constant velocity. This equation is solved by

$$q(x, t) = q_0(x - ut) \quad (2.8)$$

[Lev04, p.18], where $q_0(x) = q(x, 0)$ are the known initial conditions.

Even though this equation is very simple, its structure still resembles that of more complex problems. So its understanding plays a role at solving more difficult problems [Lev04].

Another, more complex example are the Maxwell equations

$$\begin{aligned} E_t &= \nabla \times B \\ B_t &= -\nabla \times E \end{aligned} \tag{2.9}$$

([Stu13]), which are used to describe electromagnetic fields.

In general, most problems which are solved by waves or some superposition of waves are described by hyperbolic PDEs. Of course, this also includes the description of water waves.

2.1.4 Numerical difficulties

The main problem with solving hyperbolic PDEs is to correctly handle the discontinuities that may arise in the solutions. While weak solutions can be analytically found with the criteria listed above, not all weak solutions solve the problem physically correct [Lev04, p.217]. To dismiss those incorrect solutions, the numerical methods often make use of entropy conditions (see [Lev04, chapter 11.13] for more details on this). Also it is usually not possible to simply use the differential formulation and assume it will be sufficiently smooth. Another obstacle is that the solutions often can be described as several waves of different types. The composition of types depends on the problem and has to be computed first. If the waves interact with each other, it complicates the solution further.

2.2 The shallow water equations

This thesis focuses on solving the shallow water equations, which describe water height and momentum of a fluid, in one dimension. For the shallow water equations to be applicable, the vertical scale has to be much smaller than the horizontal scale [Lev04, p.254]. This is true for ocean waves (periodic, small wavelength) and even tsunamis (caused by singular event, long wavelength, small amplitude while in deep water, high amplitude in shallow water), which are also described by the shallow water equations.

2.2.1 Equations in one dimension

The one-dimensional shallow water equations consist of two equations. The first one is:

$$h_t + (uh)_x = 0 \tag{2.10}$$

and the second one is:

$$(hu)_t + (hu^2 + \frac{1}{2}gh^2)_x = 0 \quad (2.11)$$

If $q(\vec{x}, t) = \begin{pmatrix} q_1 \\ q_2 \end{pmatrix} = \begin{pmatrix} h \\ hu \end{pmatrix}$ is introduced and $f(q) = \begin{bmatrix} hu \\ hu^2 + \frac{1}{2}gh^2 \end{bmatrix} = \begin{bmatrix} q_2 \\ (q_2)^2/q_1 + \frac{1}{2}gq_1 \end{bmatrix}$ is defined, then the equations can be written as

$$q_t + f(q)_x = 0 \quad (2.12)$$

For smooth solutions, the formulation

$$q_t + f'(q)q_x = 0 \quad (2.13)$$

is also valid [Lev04, p.254-255].

2.2.2 Properties

Since the eigenvalues and eigenvectors of $f'(q)$ are defining the entire system of equations, they are also basic properties of the problem. They have to be known to be able to compute a numeric or exact solution to any problem. They are given by ([Lev04, p.255]):

$$\lambda_1 = u - \sqrt{gh} \quad (2.14)$$

and

$$\lambda_2 = u + \sqrt{gh} \quad (2.15)$$

This leads to the eigenvectors

$$\vec{v}_1 = \begin{pmatrix} 1 \\ \lambda_1 \end{pmatrix} \quad (2.16)$$

and

$$\vec{v}_2 = \begin{pmatrix} 1 \\ \lambda_2 \end{pmatrix} \quad (2.17)$$

[Lev04, p.255].

If h is zero, both eigenvalues and thus the eigenvectors have the same value. Because the eigenvalues (and thus the eigenvectors) depend on h and u , which are the unknowns of the equation system and can be different for every point in the domain, every of these points may have different eigenvalues. It is not sufficient to compute one set of eigenvalues at the beginning and then never change it again, as can be done for the constant velocity advection equation. The eigenvalues have to be computed for each point or cell in the domain and for each time step, otherwise the numerical solution disregards the distribution in space as well as the time-development.

2.2.3 Example problems

We will look at two well known problems for the Shallow Water Equations. The first one has continuous initial conditions and is a so-called Gaussian water hump (water height is described by a Gaussian distribution). The second one is the dam break problem, a so called Riemann problem with initial velocities zero and a difference in initial height.

Riemann problems

Definition 2.2.1. A problem with initial conditions of the form

$$q(x, 0) = \begin{cases} q_l & x \leq 0 \\ q_r & 0 \leq x \end{cases}$$

is called a Riemann problem [Lev04, p.5].

The main characteristic of a Riemann problem is the discontinuity. To solve such a problem analytically, it has to be fragmented into several states. Two of them are the outer left and right states, where the solution takes the value q_l or q_r respectively. The middle states depend on the exact composition of the problem, the possibilities for the cases viewed here are either 2 shock waves, 2 rarefaction waves or one of each [Lev04, p.260]. Also a contact discontinuity often exists. In every case a middle value q_m has to be computed. The exact way to solve a Riemann problem as well as an explanation of the different types of waves will be given in chapter 3. The analytic solution for a dam-break problem will also be computed.

2.2.4 Two-dimensional equations

In two dimensions the shallow water equations can be written as ([Lev04, p.429])

$$\begin{aligned} h_t + (hu)_x + (hv)_y &= 0 \\ (hu)_t + (hu^2 + \frac{1}{2}gh^2)_x + (huv)_y &= 0 \\ (hv)_t + (huv)_x + (hv^2 + \frac{1}{2}gh^2)_y &= 0 \end{aligned} \tag{2.18}$$

This differs from the one-dimensional form by the addition of a additional dimension y . Also the velocity is now described by a vector, $\vec{u} = \begin{pmatrix} u \\ v \end{pmatrix}$. The one-dimensional equations can be derived from the two-dimensional case by setting one of the velocities to zero. The two-dimensional equations can be solved using similar techniques as for

the one-dimensional case, however for the sake of complexity this thesis will only cover the one-dimensional equations.

3 Methods for solving hyperbolic partial differential equations

There are a multitude of numerical methods to solve PDEs. However, some of them are more suited to the task of solving hyperbolic PDEs than others. As pointed out earlier some methods become unstable along discontinuities. So it's important to choose a method that handles these discontinuities well if a hyperbolic PDE has to be solved numerically.

3.1 Finite Differences

3.1.1 General description

The finite differences method is one of the better known numerical schemes. It approximates derivatives by replacing them with a difference quotient of the form

$$\frac{u(x+h) - u(x)}{h} \tag{3.1}$$

and solving the resulting equation for $u(x+h)$. The result can then be integrated by using a numerical integration scheme such as explicit Euler or other integration methods. The domain is divided into intervals of length h , for which the equation is evaluated. Higher accuracy can be achieved by choosing a smaller h . Higher order of accuracy is also possible by using a higher order integration scheme such as Runge-Kutta [BZBP13, ch. 3].

The computational domain is divided so that the method can be evaluated at certain predefined grid points.

3.1.2 Advantages and disadvantages

Advantages The method is easy to understand and since only one value is computed per interval it can also be very efficient [HW08, p.2]. Also it is possible to modify the scheme to get high order accuracy.

Disadvantages Since the finite difference becomes quite nonsensical at a discontinuity, it is not the best method for solving problems that have discontinuous initial conditions or discontinuous solutions. Also it doesn't easily allow more complex geometries, because it only supports equidistant intervals in its standard form [HW08, p.2]. While schemes with non-equidistant intervals exist, they are quite convoluted. This becomes even more of a problem for solving higher dimensional problems.

3.2 Finite Volumes

3.2.1 General description

The main difference between the method of finite volumes and the method of finite differences is that the first is based on the integral form, whereas the latter is based on the differential form [Lev04, p.5]. Using the integral form makes it possible to handle discontinuities. The computational domain is divided in cells, and for each cell the integral over this cell is approximated. For each cell, the cell average is computed, which is the quotient of the approximated integral and the cell volume [Lev04, p.5]. This means that each cell stores only this average and not an approximation polynomial or an interpolation polynomial.

To evaluate the change over time, now also fluxes from neighbor cells have to be considered. The numerical approximation to those fluxes will be explained in the following chapters.

From now on, the description will be restricted to only one dimension.
The basic idea is to describe the i -th grid cell as

$$C_i = (x_{i-1/2}, x_{i+1/2}) \quad (3.2)$$

[Lev04, p.64]. The cell average of the i -th cell in the n -th iteration can now be approximated as:

$$Q_i^n = \frac{1}{\Delta x} \int_{x_{i-1/2}}^{x_{i+1/2}} q(x, t_n) dx = \frac{1}{\Delta x} \int_{C_i} q(x, t_n) dx \quad (3.3)$$

[Lev04, p.64], where Δx is the cell size.

If this is applied to the integral formulation of a conservation law, it leads to the following equation:

$$\frac{d}{dt} \int_{C_i} q(x, t) dx = f(q(x_{i-1/2}, t)) - f(q(x_{i+1/2}, t)) \quad (3.4)$$

Since the goal is to propagate the degrees of freedom in time and thus compute the values Q_i^{n+1} at time t^{n+1} , the above equation has to be time-integrated. If the result is then divided by Δx to get the cell average, it leads to an approximation of Q_i^{n+1} .

$$\frac{1}{\Delta x} \int_{C_i} q(x, t^{n+1}) dx = \frac{1}{\Delta x} \int_{C_i} q(x, t^n) dx - \frac{1}{\Delta x} \left[\int_{t^n}^{t^{n+1}} f(q(x_{i+1/2}, t)) dt - \int_{t^n}^{t^{n+1}} f(q(x_{i-1/2}, t)) dt \right] \quad (3.5)$$

[Lev04, p.65]. Because the evolution of the flux in time is usually not known, equation (3.5) can normally not be used. Usually the time integrals over Δt are approximated by some numerical flux in the time interval Δt . The numerical flux is a linear approximation to the solution of the Riemann problem that has to be solved when evaluating the integrals at the border between two cells. These approximations lead to schemes of the following form ([Lev04, p.65]):

$$Q_i^{n+1} = Q_i^n - \frac{\Delta t}{\Delta x} (F_{i+1/2}^n - F_{i-1/2}^n) \quad (3.6)$$

$F\Delta t$ is a approximation of the time integrals in (3.5). The choice of this flux approximation heavily impacts the quality of the approximated solution. $F_{i-1/2} = F((Q_{i-1}, Q_i))$ is called a numerical flux function and it can now be seen that the approximation of Q_i^{n+1} depends on Q_{i-1} , Q_i and Q_{i+1} , a so called three point stencil [Lev04, p.66].

3.2.2 Advantages and disadvantages

Advantages One of the main benefits of the method of finite volumes is that it is stable and robust treating discontinuities. Also it is possible to use varying cell sizes, which is useful for more complex geometries [HW08, p.3]. Since the solution depends only on initial conditions and numerical fluxes one of the main tasks is to choose the numerical flux function most well-suited for the specific problem. This depends on required accuracy, stability and also on the properties of the problem itself.

Disadvantages Since only the cell average is stored for each cell, the approximation inside of one cell is quite rudimentary. It would be more accurate to give the cell more information, e.g. a value at the left boundary and the right boundary of the cell as well as a interpolation function to link those values. The inaccuracy of the cell average can of course be lessened by making the cells smaller, but it is still not as accurate (at least for continuous functions) as for example the discontinuous Galerkin method, which will be covered later.

While the method does not impose any restrictions on the choice of cell sizes and allows unstructured grids, for higher order of accuracy in higher dimensions this is no longer true (see [HW08, p.4] for more details). This means the method loses one of its main advantages. If these disadvantages are a problem for the specific problem that should be solved, and a finite difference scheme is also not the right solution, it might be necessary to take a look at finite elements methods.

3.2.3 The Courant-Friedrichs-Lewy condition

The stability of a finite volume method depends heavily on the chosen time step. If it is too big, the changed information has traveled too far and so the solution depends not only on the neighboring cells but on their neighbors etc. as well. Because those are not part of the numerical scheme the results will become increasingly wrong with time. So a condition to determine the time step size is necessary.

The Courant-Friedrichs-Lewy-condition (CFL-condition) is such a condition.

Definition 3.2.1. "A numerical method can be convergent only if its numerical domain of dependence contains the true domain of dependence of the PDE, at least in the limit as Δt and Δx go to zero"[Lev04, p.69]

The CFL condition is a necessary condition for stability and convergence. It leads to the conclusion that the Courant number

$$v = \frac{\Delta t}{\Delta x} \max |\lambda^p| \quad (3.7)$$

[Lev04, p.70] where the λ^p are the wave speeds of the system of equations, has to stay below a certain bound, usually 1 for the finite volume methods used in this thesis. From this equation the biggest time step that still leads to a stable solution can be computed by solving it for Δt . This calculation has to be repeated for every time-step to account for changes in wave speeds.

3.2.4 Flux approximations

The choice of the approximate Riemann solver is a major part of the finite volumes scheme. The following section will give short overview over some numerical flux functions. Most of these fluxes were also implemented in the program.

Unstable Flux This method follows a very simple approach by taking the average flux of both sides. The flux function is approximated by

$$F_{i-1/2}^n = \frac{1}{2} [f(Q_{i-1}^n) + f(Q_i^n)] \quad (3.8)$$

This would lead to

$$Q_i^{n+1} = Q_i^n - \frac{\Delta t}{2\Delta x} [f(Q_{i+1}^n) - f(Q_{i-1}^n)] \quad (3.9)$$

However, this approach is unstable for hyperbolic problems and all timestep sizes [Lev04, p.71].

Lax-Friedrichs flux This flux looks very similar to the unstable flux, with only an additional term added. "This additional term can be interpreted as numerical diffusion that damps the instabilities" [Lev04, p.72], that are introduced by (3.9). This makes the method stable for Courant number ≤ 1 . It has the advantage that it is still a very simple method that is easy to implement. The flux function is ([Lev04, p.71])

$$F_{i-1/2} = \frac{1}{2} [f(Q_{i-1}^n) + f(Q_i^n)] - \frac{\Delta x}{2\Delta t} (Q_i^n - Q_{i-1}^n) \quad (3.10)$$

This can then be used in (3.6) to compute the value of Q_i at the next time step. While the Lax-Friedrichs flux leads to a stable scheme the introduced diffusion is too high, as will be outlined later when the results of the Shallow Water Equations computed with this flux will be compared to the analytic solution.

The local Lax-Friedrichs-Flux The main difference between the standard Lax-Friedrichs method and the local Lax-Friedrichs method is that the factor $\frac{\Delta x}{\Delta t}$ in the computation of the fluxes is now replaced by the maximal absolute value of all wavespeeds. In particular this value is not fixed, but changes for every cell and every time. The method for determining the fluxes becomes

$$F_{i-1/2} = \frac{1}{2} (f(Q_{i-1}) + f(Q_i) - a_{i-1/2} (Q_i - Q_{i-1})) \quad (3.11)$$

[Lev04, p.232] and the factor a is determined by ([Lev04, p.233])

$$a_{i-1/2} = \max(|f(Q_{i-1})|, |f(Q_i)|) \quad (3.12)$$

For the shallow water equations this leads to the biggest eigenvalue (which are $u \pm \sqrt{gh}$) at both indexes (i and i-1 for the left side and i and i+1 for the right side). Using the local Lax-Friedrichs flux leads to better results, especially concerning centered rarefaction waves [Lev04, p.233]. This method is also known as Rusanov's method. The name "local Lax-Friedrichs method" is based on the similarity to the Lax Friedrichs method and the choice of different factors for each cell, which makes the method local.

3.3 Finite Elements

3.3.1 General description

The method of finite elements divides the domain in several elements. Even if the general geometry is very complex, the geometry of the elements is a lot simpler and makes it possible to approximate the solution inside of these elements by using local basis functions [HW08, p.5]. The approximated solution is easier to compute for a lower degree of these basis functions, but the accuracy increases with the degree of those functions. A popular choice for the basis functions are the Lagrange polynomials,

$$\ell_i^k(x) = \frac{x - x^{k+1-i}}{x^{k+1} - x^{k+1-i}} \quad (3.13)$$

It is of course possible to choose other interpolation polynomials.

The global formulation is retrieved by choosing a set of test functions that are orthogonal to the residual of the problem. For a Galerkin scheme the test functions span the same spaces as the basis functions [HW08, p.5]. Other choices of test functions are possible. For the standard advection equation this leads to a scheme of the form

$$M \frac{du_h}{dt} + Sf_h = 0 \quad (3.14)$$

where

$$M_{ij} = \int_{\Omega} N^i(x) N^j(x) dx \quad (3.15)$$

is the globally defined mass matrices (N^i are the basis functions) and

$$S_{ij} = \int_{\Omega} N^i \frac{dN^j}{dx} dx \quad (3.16)$$

is the globally defined stiffness matrix [HW08, p.6].

3.3.2 Advantages and disadvantages

Advantages Using this approach, it is possible to choose different orders of approximation in different cells [HW08, p.6] and so adapt to the specifications of the problem. Also the choice of the elements' size and geometry is very flexible.

Disadvantages However, the above choice of basis functions and the requirements they must fulfil, means that the matrix M has to be inverted and the scheme becomes implicit [HW08, p.6]. Also the choice of symmetric basis functions is not helpful for problems which prefer a certain direction, e.g. wave problems [HW08, p.6].

3.4 Discontinuous Galerkin methods

3.4.1 General description

As the previous sections show, both finite volume methods and finite element methods have some strengths, but also some weaknesses. The discontinuous Galerkin method is a method that tries to combine these strengths by using a high-order approximation like a finite elements scheme, but following the local structure of a finite volume method by using numerical fluxes at the element boundaries.

It uses the same approach of using basis and test functions to describe the solution inside an element, as well as the same elements as a finite elements method, but the nodes located on element boundaries are duplicated [HW08, p.7]. Methods with a higher number of nodes are also possible. Elements are then (in the one-dimensional case) limited to the left by x_i and to the right by x_{i+1} . For example the first cell stretches from x_0 to x_1 , while the second cell goes from x_1 to x_2 . This shows why the boundary nodes have to be duplicated: The value at the right end of cell 1 doesn't have to be the same value as the left end of cell 2. This means the solution can be discontinuous at the cell interfaces. Inside an element the solution is approximated as

$$u_h^k(x) = \sum_{i=0}^1 u^{k+i} \ell_i^k(x) \quad (3.17)$$

as well as the flux, as explained in [HW08, p.7].

To determine the test functions, the local residual (for a scalar conservation law)

$$R_h(x, t) = \frac{\delta u_h^k}{\delta t} + \frac{\delta f_h^k}{\delta x} \quad (3.18)$$

has to be orthogonal to the test functions [HW08, p.8], this means the test functions have to fulfill the following equation:

$$\int_{D^k} R_h(x, t) \ell_j^k(x) dx = 0 \quad (3.19)$$

Applying Gauss' theorem and introducing a numerical flux f^* leads to the equation [HW08, p.8]

$$\int_{D^k} R_h(x, t) \ell_j^k(x) dx = [(f_h^k - f^*) \ell_j^k]_{x^k}^{x^{k+1}} \quad (3.20)$$

Like with finite volumes, the choice of the numerical flux is an important part of the method. It is also possible to convert this equation so that it mimics the matrix formulation of finite element methods. The mass and stiffness matrices are computed analogous to this.

3.4.2 Nodal and modal formulation

There are two ways to express the solution when using a discontinuous Galerkin method. These two ways are called the nodal and the modal form [HW08, p.21].

Nodal form The nodal form uses the values at the grid points and interpolates the function between them by using some form of interpolation polynomial [HW08, p.21]:

$$u_h^k = \sum_{i=1}^{N_p} u_h^n(x_i^k, t) \ell_i^k(x) \quad (3.21)$$

In this case the interpolation polynomials are the Lagrange polynomials of order $N_p + 1$.

"The global solution $u(x, t)$ is then assumed to be approximated by the piecewise N -th order polynomial approximation $u_h(x, t)$,

$$u(x, t) \simeq u_h(x, t) = \oplus_{k=1}^K u_h^k(x, t) \quad (3.22)$$

defined as the direct sum of the K local polynomial solutions $u_h^k(x, t)$." [HW08, p.21]
Since the residual (here for the constant coefficient advection equation)

$$R_h = \frac{\delta u_h}{\delta t} + \frac{\delta a u_h}{\delta x} \quad (3.23)$$

has to be orthogonal to all test functions

$$\phi_h^k(x) = \sum_{n=1}^{N_p} \Phi_n^k \psi_n(x) \quad (3.24)$$

the following statement ([HW08, p.21]) has to be fulfilled for all $n \in [0, N_p]$:

$$\int_{D^k} R_h(x, t) \psi_n(x) dx = 0 \quad (3.25)$$

However, since this is only a local statement, it doesn't help in finding the global solution. Spatial integration and the choice of a sensible numerical flux $(au_h)^*$ (see [HW08, p.22]) leads to the weak form ([HW08, p.22])

$$\int_{D^k} \left(\frac{\delta u_h^k}{\delta t} \psi_n - a u_h^k \frac{\delta \psi_n}{\delta x} \right) dx = - \int_{\delta D^k} \hat{n} \cdot (au_h)^* \psi_n dx \quad (3.26)$$

and the strong form ([HW08, p.22])

$$\int_{D^k} R_h(x, t) \psi_n(x) dx = \int_{\delta D^k} \hat{n} \cdot (a u_h^k - (au_h)^*) \psi_n dx \quad (3.27)$$

where \hat{n} is the outward pointing normal (+1 and -1 for one dimension) [HW08, p.22] and $(au_h)^*$ is a chosen numerical flux function.

For a mass matrix

$$\hat{M}_{ij}^k = \int_{D^k} \ell_i \ell_j dx \quad (3.28)$$

and stiffness matrix

$$\hat{S}_{ij}^k = \int_{D^k} \ell_i \frac{d\ell_j}{dx} dx \quad (3.29)$$

the weak form can be written as

$$\hat{M}^k \frac{d}{dt} u_h^k - (\hat{S})^T a u_h^k = -(au_h)^* \psi(x_r^k) + (au_h)^* \psi(x_l^k) \quad (3.30)$$

and the strong form as

$$\hat{M}^k \frac{d}{dt} u_h^k + \hat{S}^k a u_h^k = (au_h^k - (au_h)^*) \psi(x_r^k) - (au_h^k - (au_h)^*) \psi(x_l^k) \quad (3.31)$$

(see [HW08, p.23-24]).

Modal form The modal form uses a local polynomial basis [HW08, p.20]:

$$u_h^k(x, t) = \sum_{n=1}^{N_p} \hat{u}_n^k(t) \psi_n(x) \quad (3.32)$$

where $\psi_n(x)$ is the polynomial basis function and N_p is the polynomial order plus one. Following the same approach as above to determine the weak and strong forms for test functions that have the same space as the solution space (called a Galerkin approach) [HW08, p.23] leads to the same equations as (3.30) and (3.31) with local mass matrix

$$\hat{M}_{ij}^k = \int_{D^k} \psi_i \psi_j dx \quad (3.33)$$

and local stiffness matrix

$$\hat{S}_{ij}^k = \int_{D^k} \psi_i \frac{d\psi_j}{dx} dx \quad (3.34)$$

[HW08, p.23].

3.4.3 Handling more complex equations

The explanations until now only used a very basic linear flux function au and only one unknown. If we assume that the flux is given by some flux function $f(u)$, we can use the same equations ((3.27) and (3.26)) for the weak and strong formulation, but

now au_h^k is replaced by $f_h^k(u_h^k)$ (which is also defined as a sum of coefficients and basis functions) and $(au_h)^*$ by f^* :

$$\int_{D^k} \left(\frac{\delta u_h^k}{\delta t} \psi_n - f_h^k(u_h^k) \frac{\delta \psi_n}{\delta x} \right) dx = - \int_{\delta D^k} \hat{n} \cdot f^* \psi_n dx \quad (3.35)$$

$$\int_{D^k} \left(\frac{\delta u_h^k}{\delta t} + \frac{\delta f_h^k(u_h^k)}{\delta x} \right) \psi_h^k dx = \int_{\delta D^k} \hat{n} \cdot (f_h^k(u_h^k) - f^*) \psi_h^k dx \quad (3.36)$$

[HW08, p.31] The generalization into more than one dimension leaves this structure intact, the scalars for u , \hat{n} and f get replaced by their vector equivalents and the space derivative gets replaced by the gradient (weak form) or the divergence (strong form) [HW08, p.34].

3.4.4 Advantages and disadvantages

Advantages The discontinuous Galerkin method makes it possible to achieve high order of accuracy even on unstructured grids. Also it can make use of different flux functions, making it possible to choose a flux tailored to the specific problem that shall be solved [HW08, p.9]. Choosing the right flux makes it also possible to reduce oscillations in comparison with finite element methods [HW08, p.9].

Disadvantages The computational effort is a lot higher than for simpler methods. This is caused by the doubling of the nodes but also by the more complex numerical computation. Especially with high-order interpolation and thus bigger matrices to compute, this is an issue [HW08, p.9]. Also, of course, for problems that don't need the advantages of the discontinuous Galerkin method and are not hit especially hard by the weaknesses of other methods, this computational effort is often not worth it.

3.4.5 Comparison between the methods

The following figure (source [HW08, p.7]) gives an overview over the strengths and weaknesses of each of the methods analyzed so far. It can be seen that the discontinuous Galerkin method is a good combination of the strengths of finite volume methods and finite element methods, because it combines possible high order of accuracy with an explicit semi-discrete form.

Figure 3.1: Comparison of the advantages and disadvantages of different methods (FDM = finite differences, FVM = finite volumes, FEM = finite elements, DG-FEM = discontinuous Galerkin) to solve hyperbolic PDEs, source [HW08, p.7]

	Complex geometries	High-order accuracy and hp -adaptivity	Explicit semi-discrete form	Conservation laws	Elliptic problems
FDM	×	✓	✓	✓	✓
FVM	✓	×	✓	✓	(✓)
FEM	✓	✓	×	(✓)	✓
DG-FEM	✓	✓	✓	✓	(✓)

3.5 Summary of numerical integration methods

The following section aims to give a short overview over the most common time integration methods and their usage without going too much into detail.

3.5.1 Explicit Euler

For a given $\frac{d}{dt}x = f(t, x)$ with initial value $x(t_0) = x_0$, the explicit Euler step is

$$x_{n+1} = x_n + hf(t_n, x_n) \quad (3.37)$$

where h is the time step size.

While this method is simple to use, it doesn't suit all kinds of numerical problems. Especially problems with high stiffness prefer an implicit method [BZBP13]. Also more accurate schemes exist. When using an explicit euler step, the time step size is also limited by the CFL-condition (has to be lower than 1).

Improved explicit Euler - midpoint method A simple way to improve explicit Euler methods is by first computing a middle step for x

$$x_{n+1/2} = x_n + \frac{h}{2}f(t_n, x_n) \quad (3.38)$$

and then using this to compute the corresponding value of $f(x, t)$ and use it to get the final value of the full time step ([BZBP13])

$$x_{n+1} = x_n + hf(t_{n+1/2}, x_{n+1/2}) \quad (3.39)$$

3.5.2 Implicit Euler

Used especially for problems of high stiffness, the implicit euler step is defined as

$$x_{n+1} = x_n + hf(x_{n+1}, t_{n+1}) \quad (3.40)$$

. This method needs more computational effort because for each time step a equation system has to solved for x_{n+1} , because both sides of the equation depend on x_{n+1} . This means $f(x, t)$ has to be inverted each time step. The implicit euler method is not restricted in its time step size by the CFL condition, because it is A-stable, so this may be worth it for some problems [BZBP13]. The implicit Euler method has order of convergence one.

3.5.3 Heun's method

To get a higher rate of convergence (the euler methods have 1, Heun's method has 2) a temporary value \tilde{x}_{k+1} is computed. The complete method is then given by ([BZBP13])

$$\begin{aligned} \tilde{x}_{n+1} &= x_n + hf(x_n, t_n) \\ x_{n+1} &= x_n + \frac{1}{2}h(f(t_n, x_n) + f(t_{n+1}, \tilde{x}_{n+1})) \end{aligned}$$

The disadvantage of this method is that for each time step two values have to be computed.

3.5.4 Runge-Kutta methods

Runge-Kutta methods are a family of methods with varying number of middle values per timestep and explicit as well as implicit forms. The most common Runge-Kutta method has four middle values and is explicit. It has the form ([BZBP13])

$$x_{k+1} = x_k + h \cdot \frac{1}{6}(k_1 + 2k_2 + 2k_3 + k_4) \quad (3.41)$$

with

$$\begin{aligned} k_1 &= f(x_n, t_n) \\ k_2 &= f(x_n + \frac{h}{2}k_1, t_n + \frac{h}{2}) \\ k_3 &= f(x_n + \frac{h}{2}k_2, t_n + \frac{h}{2}) \\ k_4 &= f(x_n + hk_3, t_n + h) \end{aligned}$$

With this method, a rate of convergence of four is possible, but at the cost of having to compute four extra values per time step. For a discontinuous Galerkin approach this means that for each of those middle values the domain has to be traversed again and a new value for f has to be computed.

4 Analytic solution of the dam-break problem

To evaluate how well the numerical methods used for solving the dam-break problem in the implementation work and how they compare to each other, we need to know the exact solution for this problem. The following section will explain how to solve a given Riemann problem for the shallow water equations. The specific solution for the problem used in the implementation will be computed based on this knowledge in the next chapter.

4.1 Introduction

As defined earlier in (2.2.1), a Riemann problem is a special set of initial conditions, where the initial velocities are zero over the whole domain and the height is piece-wise constant, with a left and a right starting height, as in (2.2.1).

Because the solution stays constant along characteristics [Lev04, p.19], the solution can be divided into several areas with identical behavior. Two of those sections are areas where the water has still the height before the waves reach it (so the smaller of h_l and h_r) and behind the waves where the height is still the bigger one. What happens between those boundaries depends on the properties of the problem, more precisely on which types of waves occur in which order. For the dam-break problem as defined above, the solution always contains one shock wave and one rarefaction wave [Lev04, p.260].

4.1.1 Shock waves

Physically, a shock wave is a wave traveling faster than the speed of sound of the fluid it travels in. It is characterized by a sudden change of value of the examined variables. A well known example is the sonic boom observed when aircraft travel faster than the speed of sound in air. A shock wave also occurs at the end of a traffic jam, where cars' velocity changes abruptly from some positive value to zero. In the case of the shallow water equations, shock waves are discontinuities in height and/or velocity that travel through the water [Lev04, p.203].

4.1.2 Rarefaction waves

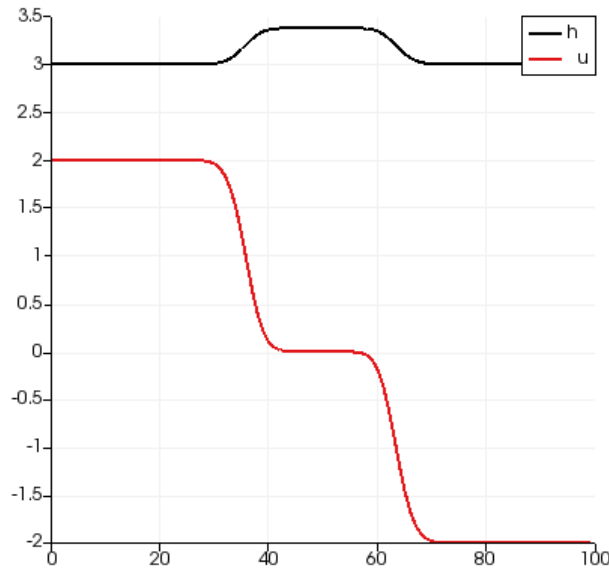
Rarefaction waves are defined by a gradual increase or decline of (in our case) height and/or velocity [Lev04, p.206], in contrast to the sudden changes associated with shock waves. Classically, they occur behind a traveling shock wave. They usually widen and spread out over time.

4.2 Different types of wave composition

4.2.1 Two shocks

If the initial height is uniform over the whole domain and the velocity is piece-wise constant with $u_r = -u_l$, the solution consists of two shock waves [Lev04, p.262]. The

Figure 4.1: Two shocks - Paraview visualization of a numerical approximation to a problem with $u_l = 2$, $u_r = -2$ and $h_0 = 3$ at time $t \approx 2.65$ for a computational domain of size 100, horizontal axis x position, vertical axis h and u

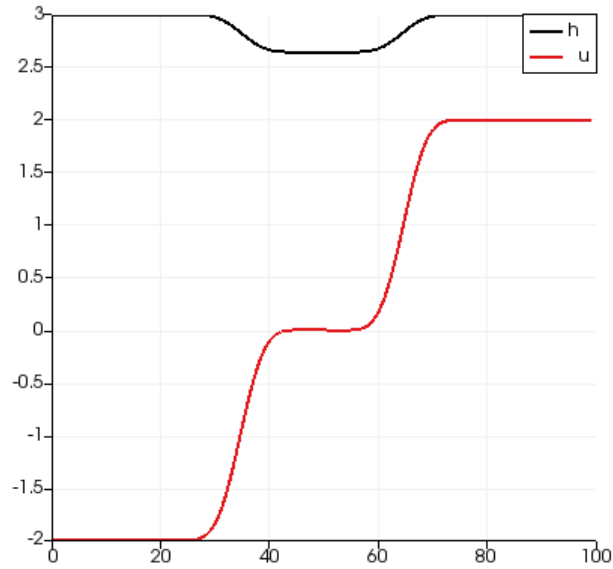


approximated shock waves can be seen, especially in the steep declines in u . The left shock travels to the left and the right shock to the right.

4.2.2 Two rarefaction waves

While the example for two shock waves can be explained as two bodies of water colliding, two bodies of water that travel away from each other lead to a solution consisting of two rarefaction waves [Lev04, p.277]. To achieve this, the sign of the velocities used in 4.1 have to be reversed. Since the figures were made from a numerical approximation using a finite volume scheme the difference between the shocks and rarefaction waves is not as strong as in an exact solution.

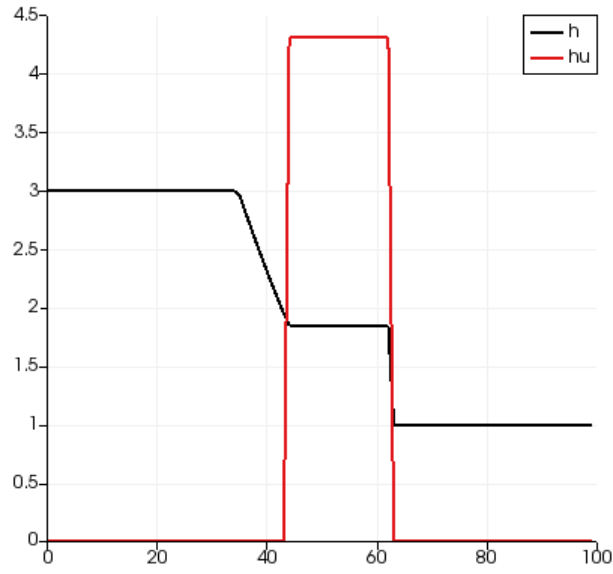
Figure 4.2: Two rarefaction waves - Paraview visualization of a numerical approximation to a problem with $u_l = -2$, $u_r = 2$ and $h_0 = 3$ at time $t \approx 2.65$ for a computational domain of size 100, horizontal axis x position, vertical axis h and u



4.2.3 One rarefaction wave and one shock

The problem that is solved in the implementation section is solved by a combination of a shock and a rarefaction wave. The shock travels to the right and the abrupt change in height is clearly visible.

Figure 4.3: 1 rarefaction, 1 shock - Paraview visualization of the exact solution to a problem with $u_l = u_r = 0$, $h_l = 3$ and $h_r = 1$ at time $t \approx 2.65$ for a computational domain of size 100, horizontal axis x position, vertical axis h and hu



4.3 Solving the problem

In all types of wave composition, the solution can be split in five sections. The first is, as already discussed earlier, the area behind the wave. In figure 4.3 this is the left section with $h = h_l$. There is also an area in front of the wave, in 4.3 this is the section with $h = h_r$. Between those two areas waves impact the variables. Each of them defines the behavior in one section. Between waves there is some middle state with properties that depend on the initial problem.

To find an exact solution, the first step is to find what types of waves occur in the given scenario [Lev04, p.263]. To do this, an entropy condition like the Lax condition, which gives requirements for a shock wave, can be used [Lev04, p.285]. In general, the solution has to fulfill certain admissibility conditions. These prohibit non-physical weak solutions [Lev04, p.217]. As mentioned earlier, it can be shown that the solution is constant along rays of x/t . For each ray the wave it belongs to has to be determined. The third step is then to compute the middle state q_m between the two waves [Lev04, p.263].

4.3.1 Determining the boundaries of each section

One of the main characteristics of a Riemann problem is that its solution is constant along rays of x/t . This can be used to determine different parts of the solution. If the solution has two shock waves, both outer areas have to have wave speeds higher than their respective shock speed [Lev04, p.262]. If there are two rarefaction waves, the outer areas have a slower wave speed than their respective rarefaction [Lev04, p.279]. If the solution contains one of each type of waves, one of the areas not affected by the waves is the one behind a rarefaction wave, this means that for these x values the wave speed of the neighbouring rarefaction is higher than x/t . The same consideration can be used for the areas in front of shocks. For those areas x/t has to be faster than the shock speed [al.16]. If the solution consists of two shocks, these boundaries are sufficient to solve the problem, since the shock waves are discontinuities and thus occur at exactly one x . If the solution has rarefaction waves, if x/t is between the outer wave speed and the middle state wave speed, it is in the area of the rarefaction wave. If x/t is faster than the speed of the left wave, but slower than the right wave (or the other way around for solutions traveling to the right) it lies within the section of the middle state.

4.3.2 Getting the middle state

The height and velocity of the middle state q_m depends on the heights and velocities of the left and right state. If a shock is present, the system of equations arising from the

Rankine-Hugoniot condition can be used to compute the middle state [Lev04, p.265]. For a solution consisting of two shocks, this is sufficient and gives the physically correct solution.

4.3.3 Computing the shock speed

The shock speed is given by the Rankine-Hugoniot condition [Lev04, p.265] and depends on the values of the two states in front and behind the shock. This is described by the equation

$$s = \frac{h_* u_* - h u}{h_* - h} \quad (4.1)$$

and if assumed, for example, that the shock is between the middle and the right state, $h_* = h_m$ and $h = h_r$.

4.3.4 Determining the behaviour inside a rarefaction wave

The behaviour of a rarefaction wave can be described by a centered wave. These are a type of simple waves, which means they can be described by scalar nonlinear equations [Lev04, p.269]. They are of the following form:

$$q(x, t) = \begin{cases} q_l & x/t \leq \xi_1 \\ \tilde{q}(x, t) & \xi_1 \leq x/t \leq \xi_2 \\ q_r & x/t \geq \xi_2 \end{cases} \quad (4.2)$$

q_l and q_r are some states separated by a rarefaction wave, where q_l has a lower wavespeed than q_r [Lev04, p.276]. The exact process to compute \tilde{h} is given in [Lev04, p.277]. A detailed explanation is also given in [Sto57], chapter 10, especially 10.8. It uses the fact that q_m has to lie on specific integral curves. It results in

$$\tilde{h} = \frac{1}{9g}(A - \xi)^2 \quad (4.3)$$

with

$$A = u_l + 2\sqrt{gh_l} = u_r + 2\sqrt{gh_r} \quad (4.4)$$

This means the evolution of h inside the rarefaction wave is described by a parabolic curve.

To compute u the value for \tilde{h} has to be put in the following equation

$$u = u_* - 2(\sqrt{gh_*} - \sqrt{gh}) \quad (4.5)$$

[Lev04, p.271].

4.3.5 Putting the solution together

Now all values and all boundaries of areas are known. The final solution is then given by defining a piecewise defined function that takes all the information computed before into consideration. [al.16] gives a compact overview over all kinds of analytic solutions for the shallow water equations in one and two dimensions. For a problem with initial conditions similar to figure 4.3 they give the solution, consistent with the solving process described above, as

$$h(x, t) = \begin{cases} h_l & x/t \leq \lambda_{1l} \\ \frac{4}{9g}(\sqrt{gh_l} - \frac{1}{2}(x/t))^2 & \lambda_{1l} \leq x/t \leq \lambda_{1m} \\ h_m & \lambda_{1m} \leq x/t \leq s \\ h_r & x/t > s \end{cases} \quad (4.6)$$

$$u(x, t) = \begin{cases} u_l & x/t \leq \lambda_{1l} \\ \frac{2}{3}((x/t) + \sqrt{gh_l}) & \lambda_{1l} \leq x/t \leq \lambda_{1m} \\ u_m & \lambda_{1m} \leq x/t \leq s \\ u_r & x/t > s \end{cases} \quad (4.7)$$

The equations given in [Sto57, chapter 10.8] also lead to the same piece-wise defined function. For a solution consisting only of shocks or only of rarefaction waves, the values and boundaries would be different, according to the above explanations.

5 Implementation

For this thesis, a program containing a finite volume solver (with several numerical flux options) and a discontinuous Galerkin for the simple advection equation and the shallow water equations was implemented. Building further upon the theoretical concepts in chapters 2 and 3, in this chapter the details of this implementation will be described and the results will be compared against theoretical values. Also the behaviour of the error will be examined and the order of convergence for the different methods determined.

5.1 Computed scenarios

Two types of initial conditions were used, one of them continuous and one discontinuous. Continuous initial conditions were primarily used for solving the advection equation, the discontinuous case is a classic use case for the shallow water equations. To be able to compare results, the same initial conditions were used for the finite volumes solver as well as for the discontinuous Galerkin solver.

5.1.1 Continuous initial conditions - Gaussian distribution

As an example of continuous initial conditions, a water hump with gaussian height distribution was used. The water height (for the advection equation it might also be some density or similar) is described by a gaussian distribution

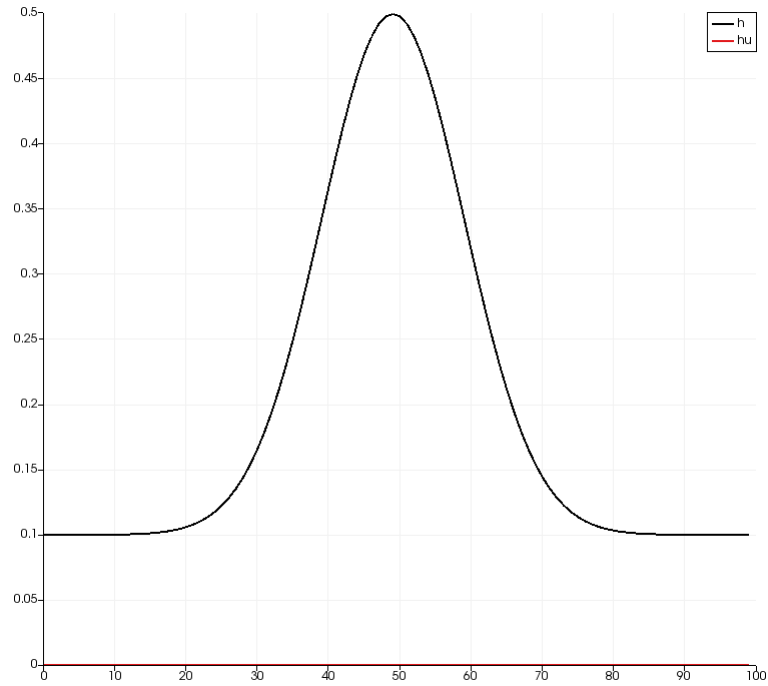
$$f(x) = \frac{1}{\sqrt{2\pi\sigma^2}} e^{-\frac{(x-\mu)^2}{2\sigma^2}} \quad (5.1)$$

with $\sigma = 10$, $\mu = 0$ and $x = pos - x_0$, where $pos = \Delta x i$ is the product of cell size Δx and number of interval i and x_0 is the middle of the computational domain. So the height distribution is given by

$$h(x) = \frac{1}{\sqrt{200\pi}} e^{-\frac{x^2}{200}} \quad (5.2)$$

This height is then multiplied by 10 and added to a basic height of 0.1 to prevent the water height becoming zero, where the shallow water equations are no longer valid, and disturbing the calculations by using incorrect negative values, which might lead to uncontrolled oscillations. The water hump then has its maximum at the middle of the domain with a corresponding height of ≈ 0.5 .

Figure 5.1: Paraview visualization of the initial conditions following a Gaussian distribution for a computational domain of size 100



Boundary conditions For the advection equation periodic boundary conditions were used. Since for these boundaries the solution is periodic, it is possible to use this fact to compute the error over time (for the time where the maximum reaches its initial location for the n -th time) by simply comparing it with the starting conditions. For the shallow water equations the boundary elements were simply estimated by their direct neighbour and thus the boundary conditions were not periodic.

5.1.2 Discontinuous initial conditions - dam-break problem

To test the numerical solution's ability to handle discontinuities, a discontinuous test case was used. This was a classical dam-break problem with initial values

$$h(x,0) = \begin{cases} 3 & x \leq x_0 \\ 1 & x_0 \leq x \end{cases} \quad (5.3)$$

$$hu(x,0) = 0 \quad (5.4)$$

with x_0 defining the middle of the computational domain.

This defines a divided area of water, where the left half has height 3 and the left half has height 1.

For this dam-break problem an analytic solution can be found, as given in 5.1.3. This can then be used to compute an error to test the accuracy of the used numerical methods.

Figure 5.2: Paraview visualization of the initial conditions of the used dam-break problem for a computational domain of size 100



Boundary conditions Like for the shallow water solution for the Gaussian bump, non-periodic boundary conditions were used that simply extrapolate from their direct neighbour.

5.1.3 Exact solution of the used dam-break problem

The exact solution for the used dambreak problem 5.3 can be computed by using equations (4.6) and (4.7) and the given values for h and u . The necessary wavespeeds are

$$\begin{aligned}\lambda_{1l} &= u_l - \sqrt{gh_l} = -5.423991150 \\ \lambda_{1m} &= u_m - \sqrt{gh_m} = -1.92517691 \\ s &= (hu_m - hu_r)/(h_m - h_r) = 5.081313902\end{aligned}$$

The middle state has the following values:

$$\begin{aligned}h_m &= 1.848576603 \\ u_m &= 2.332542824\end{aligned}$$

All equations were solved with and the values computed with Maple. This leads to the following analytic solution:

$$h(x, t) = \begin{cases} 3 & x/t \leq \lambda_{1l} \\ \frac{4}{9g}(\sqrt{3g} - (x/2t))^2 & \lambda_{1l} \leq x/t \leq \lambda_{1m} \\ h_m & \lambda_{1m} \leq x/t \leq s \\ 1 & x/t > s \end{cases} \quad (5.5)$$

$$u(x, t) = \begin{cases} 0 & x/t \leq \lambda_{1l} \\ \frac{2}{3}((x/t) + \sqrt{3g}) & \lambda_{1l} \leq x/t \leq \lambda_{1m} \\ u_m & \lambda_{1m} \leq x/t \leq s \\ 0 & x/t > s \end{cases} \quad (5.6)$$

5.2 Details of implementation

5.2.1 General information

The program is based on the SWE1D program by Sebastian Rettenberger [Ret]. While none of the original solvers are still used, the basics of the main program remain

unchanged. All implementation was done in C++. The program can be built either with CMake or with SCons. Source code is available at this [GitHub](#) page. The output from the numerical computations can be visualized using ParaView, using either the "Plot Data" filter (for all finite volume solvers) or "Plot Over Line" for discontinuous Galerkin solvers.

While it can be run using command line parameters for number of intervals and number of time steps (e.g. `-s 1000 -t 300` for 1000 space intervals and 300 time steps), it is also possible to manipulate the default parameters inside `args.h`. The default settings use a finite volume solver in combination with local Lax-Friedrichs flux, a domain size of 100 and 100 time steps. The very beginning of `main.cpp` contains some boolean variables that function as switches for the different solvers and scenarios.

5.2.2 Switches to use finite volume methods

bool SWE This boolean is set to true if some scenario shall be computed using the shallow water equations, using a finite volume method.

bool Adv This boolean is used to set the used equations to the advection equation (simplest form with constant wave speed).

bool dambreak This boolean is set additionally to SWE for a dam break scenario that shall be solved using finite volume methods.

bool gauss This boolean can be used either with SWE or with Adv, depending if the evolution of the Gaussian hump given in (5.1) shall be solved for the shallow water equations or for the advection equation. Used only for finite volume methods.

5.2.3 Switches to use discontinuous Galerkin methods

bool AdvDG This is set to true to solve the advection equation with a discontinuous Galerkin scheme.

bool SWEDG This boolean is used to solve the shallow water equation for the dam break problem given earlier.

bool SWEDGGAuss If this is set to true, the shallow water equations will be solved for a Gaussian water hump.

bool improvedEuler If this is set to true, then instead of an explicit Euler integration scheme, the midpoint method will be used.

5.2.4 Other switches

bool errorComputing If this is set to true, the error of the used method will be computed. For the advection equation, the initial condition will be saved and compared to the numerical solution after the maximum of the Gaussian distribution reaches its origin again. For the shallow water equations, the error will only be computed for a dam break scenario. At a predefined time (currently set to 0.5s), the exact solution will be computed using the equations (5.5) and (5.6). This can then be compared to the numerical solution. If error computing is active, no vtk output will be written. The time steps needed to reach the point where an error can be computed will also be computed and overwrite the given number of time steps. This is especially important for a very high number of intervals or very small CFL numbers.

5.3 Used methods

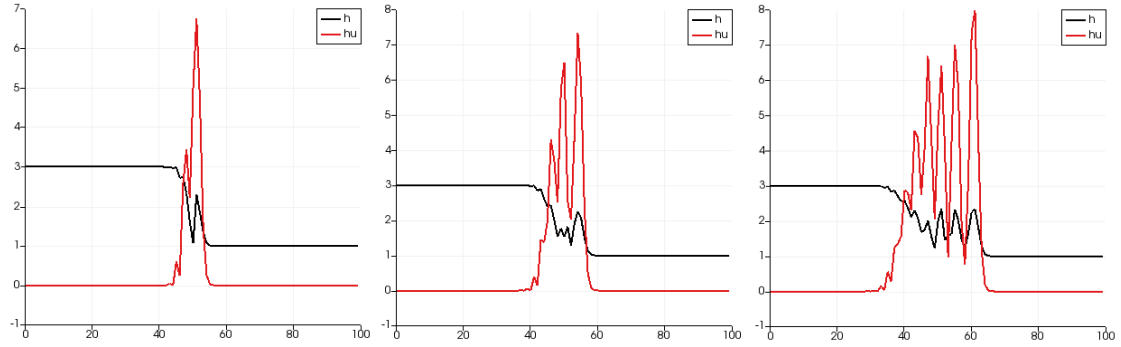
5.3.1 Finite Volumes

All finite volume methods use the same process. First the boundary values are set (either to periodic or neighbour values, depending on the scenario). Then, for each cell, the numerical fluxes from the left and right neighbour are computed. In this step, the new time step size is also computed from the CFL condition. After that, the values of the fluxes are used to compute the new values of q . Afterwards, the results are given to the vtk writer and written to a file.

Numerical fluxes

Unstable flux The method described in equations (3.8) and (3.9) is implemented using those equations, with Courant number 0.4. Figure 5.3 shows the increasing oscillations over time (soon after this they start to amplify with every time step and completely dominate the results) and thus this numerical flux function is not suitable for hyperbolic PDEs, as already said earlier.

Figure 5.3: Evolution of the solution to the dam break problem using an unstable flux, $t=1.4$, $t=2.7$ and $t=5.2$



Lax-Friedrichs flux Equations (3.10) and (3.6) are used to implement the classical Lax-Friedrichs flux. While the results, visible in figure 5.4 and figure 5.5, don't show oscillations anymore, they show noticeable differences from the analytic solution. In particular, the two waves that form in the middle of the dam-break area are computed overly smooth and are barely distinguishable.

Figure 5.4: Evolution of the solution of the dam break problem using Lax-Friedrichs flux, $t_1=1.4$, $t_2=2.7$, $t_3=5.2$

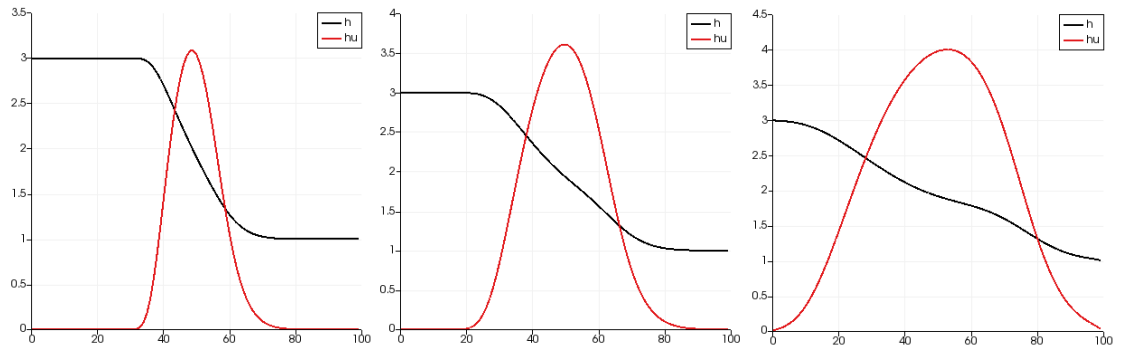
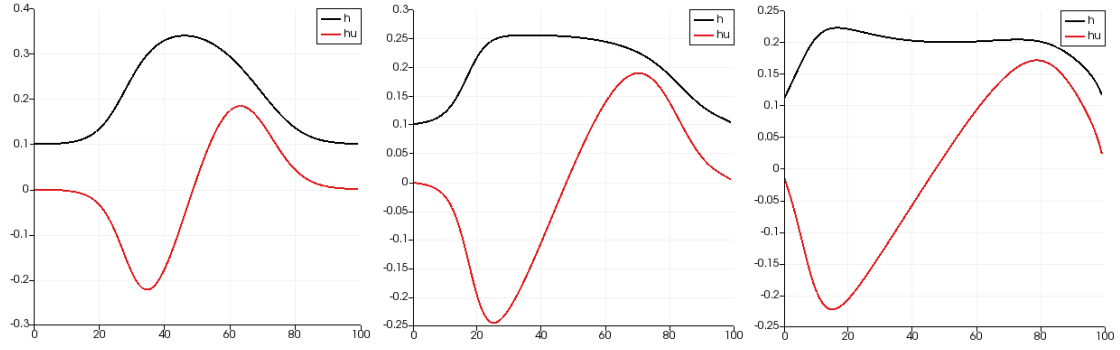


Figure 5.5: Evolution of the solution of the gaussian water hump using Lax-Friedrichs flux, $t_1=5.4$, $t_2=10.1$, $t_3=15.3$



Local Lax-Friedrichs flux The local Lax-Friedrichs flux is implemented using (3.11) for a Courant number of 0.4. This method clearly shows the best results, as shown in 5.6 and 5.7. The solution doesn't show any kind of unwanted oscillations and is also able to handle the discontinuity in the dam break problem well.

Figure 5.6: Evolution of the solution of the dam break problem using a local Lax-Friedrichs flux, $t_1=1.4$, $t_2=2.7$, $t_3=5.2$

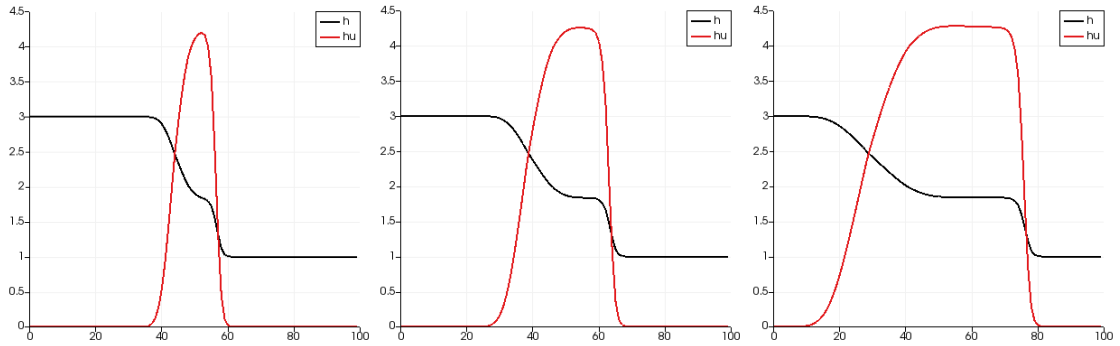
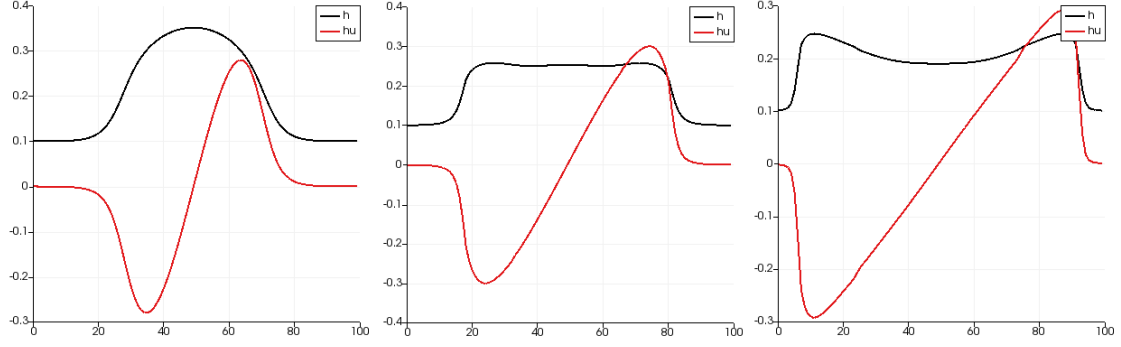


Figure 5.7: Evolution of the solution of the gaussian water hump using a local Lax-Friedrichs flux, $t_1=5.4$, $t_2=10.1$, $t_3=15.3$



5.3.2 Discontinuous Galerkin

While results using finite volume methods improved through the use of better numerical flux functions, they still differ significantly from the exact solution. For example, discontinuities in the exact solution are computed too smooth and with slope too shallow. To get results closer to the exact solution, a discontinuous Galerkin scheme was implemented.

The process for the discontinuous Galerkin methods is similar to the one for finite volume methods, except that instead of computing the new values for q directly from the old values and numerical fluxes, the fluxes are used to compute the time-derivative, which is then used to compute the new values for each node, using a time-integration method (in this case an explicit Euler step). After this, the values of q are given to a vtu writer and written to a file.

The numerical flux used is a local Lax-Friedrichs flux. The local test functions, as well as the basis functions, are the Lagrange polynomials of degree 1 over the basis interval from 0 to 1. So $\varphi_0(x) = 1 - x$ and $\varphi_1(x) = x$.

Advection equation For the simple advection equation (one dimension, fixed speed), the following equation has to be solved:

$$u_t + au_x = 0 \quad (5.7)$$

For each interval, this means the following has to be true:

$$\forall i \in 1 \dots N \int_{I_i} \varphi_i(x)(u_t + au_x) = 0 \quad (5.8)$$

Sine we use a nodal representation, this leads to the following:

$$\forall i \in 1...N \int_{I_i} \varphi_i \left(\sum_j (\varphi_j u_j)_t + a \sum_j (\varphi_j u_j)_x \right) dx = 0 \quad (5.9)$$

To get an expression for u_t above expression has to be manipulated accordingly, using the fact that φ does not depend on t and u_j doesn't depend on x . Partial integration is also used to get an expression for the integral containing the space derivative $\int_{I_i} \varphi_i (\varphi_j)_x u_j dx$. The manipulations lead to

$$\begin{aligned} \forall i \in 1...N : \\ \sum_j \int_{I_i} \varphi_i \varphi_j (u_j)_t dx - a \int_{I_i} \varphi_j u_j (\varphi_i)_x dx + (\varphi_i \varphi_j)|_{x_l} ((au)^*)_l - (\varphi_i \varphi_j)|_{x_r} ((au)^*)_r = 0 \end{aligned}$$

A complete derivation is given in appendix 1. This can be put into matrix form known from chapter 3. It is important to remember that u is in fact a vector, containing two nodes for each cell $u = \begin{pmatrix} u_0 \\ u_1 \end{pmatrix}$.

$$M \Delta x u_t - S \Delta x (au) + N_0 f_l - N_1 f_r = 0 \quad (5.10)$$

This leads to the wanted equation for u_t :

$$u_t = (M^{-1} \cdot (S(au) + N_0 f_l - N_1 f_r)) / \Delta x \quad (5.11)$$

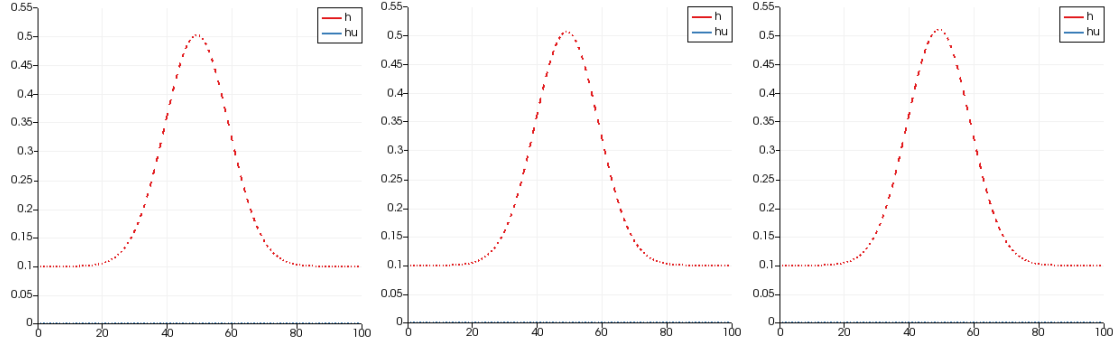
f_l and f_r are the fluxes from left or right, computed with a local Lax-Friedrichs approximation. The matrices are (instead of evaluating the specific interval, the transformation theorem can be used to use the basis interval from 0 to 1 instead):

$$\begin{aligned} M &= \begin{pmatrix} \frac{1}{3} & \frac{1}{6} \\ \frac{1}{6} & \frac{1}{3} \end{pmatrix} M^{-1} = \begin{pmatrix} 4 & -2 \\ -2 & 4 \end{pmatrix} \\ S &= \begin{pmatrix} -\frac{1}{2} & -\frac{1}{2} \\ \frac{1}{2} & \frac{1}{2} \end{pmatrix} N_0 = \begin{pmatrix} 1 & 0 \\ 0 & 0 \end{pmatrix} N_1 = \begin{pmatrix} 0 & 0 \\ 0 & 1 \end{pmatrix} \end{aligned}$$

The explicit Euler step is then given by

$$u^{n+1} = u^n + \Delta t u_t \quad (5.12)$$

Figure 5.8: DG approximation (advection equation) after 1, 2 and 3 full "circles"



Visualization of results Figure 5.8 shows the results for the advection equation after one, two and three turnarounds. The solution shows no significant dissolution or shape change, and thus gives correct results even for later times.

Shallow water equations Since the shallow water equations are a system of two hyperbolic PDEs, the derivation of u_t , as done above for the advection equation, has to be done twice, once for each equation. While the advection equation used the very simple flux au , now the equations use a flux function $f(q)$, as defined in chapter 2.2.1. This doesn't change the structure of the result, but $S(au)$ becomes $Sf(h)$ for the equation for h and $Sf(hu)$ for the equation for hu . Of course, the left and right fluxes also use the corresponding flux function and not the one from the advection equation.

Visualization of results Figure 5.9 shows the results for the shallow water equations after one, two and three turnarounds for a dam break problem and figure 5.10 shows the results for a Gaussian water hump.

Figure 5.9: DG approximation (SWE, dam break) $t_1=1.4$, $t_2=2.7$, $t_3=5.2$

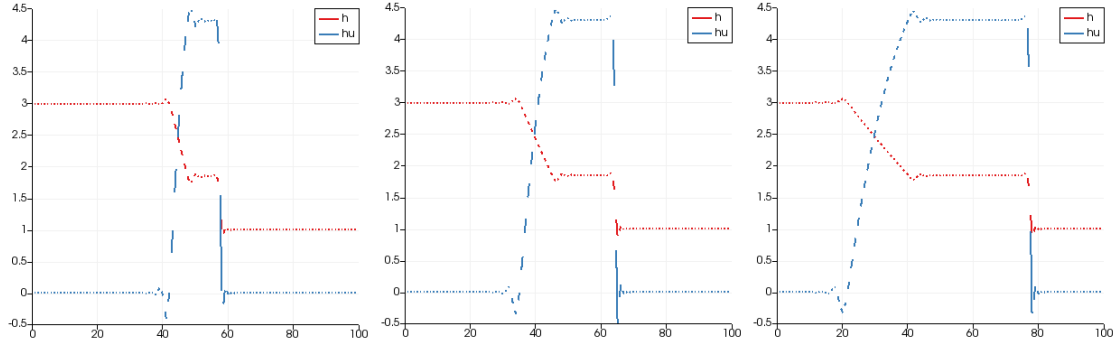
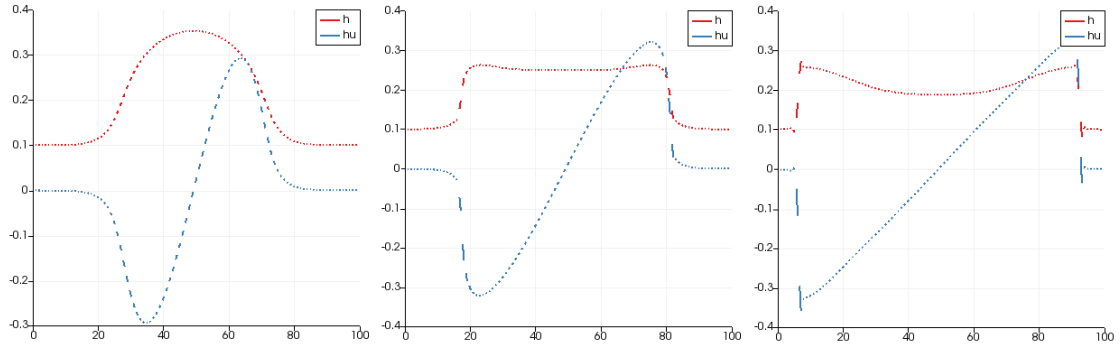


Figure 5.10: DG approximation (SWE, gaussian) $t_1=5.4$, $t_2=10.1$, $t_3=15.3$



5.4 Comparison of finite volume and discontinuous Galerkin

5.4.1 Advection equation

If the time evolution of the advection solution is computed using a finite volume scheme, it contains too much dissipation. The expected result would be a wave of unchanging shape traveling at the given wave speed, since the model contains no friction losses. However, the wave maximum decreases noticeably over time and the shape also doesn't stay the same (visualized in figure 5.11).

If the approximation computed by a discontinuous Galerkin solver is evaluated at the same time, these dissipation effects don't occur at all, neither in height nor in shape (see figure 5.12).

A direct comparison between the two methods (same size of domain and same

Figure 5.11: Finite volume approximation (advection equation) after 1, 2 and 3 full "circles"

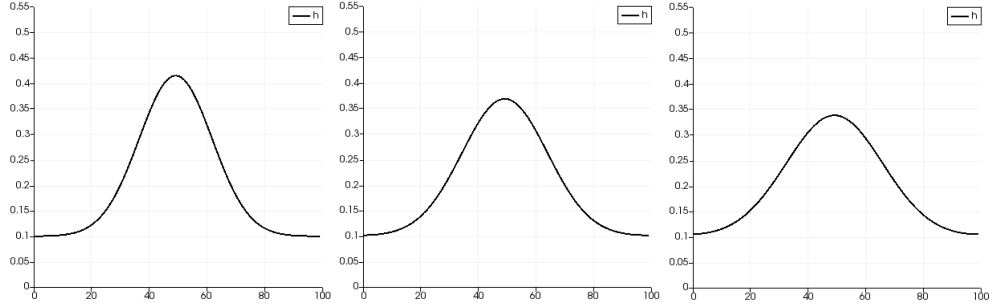
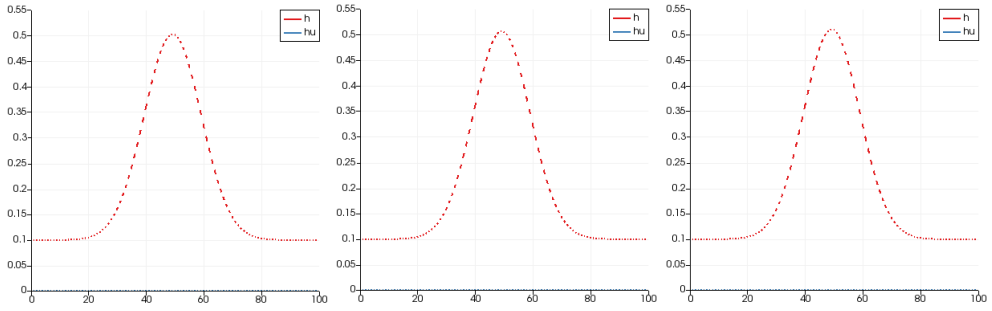
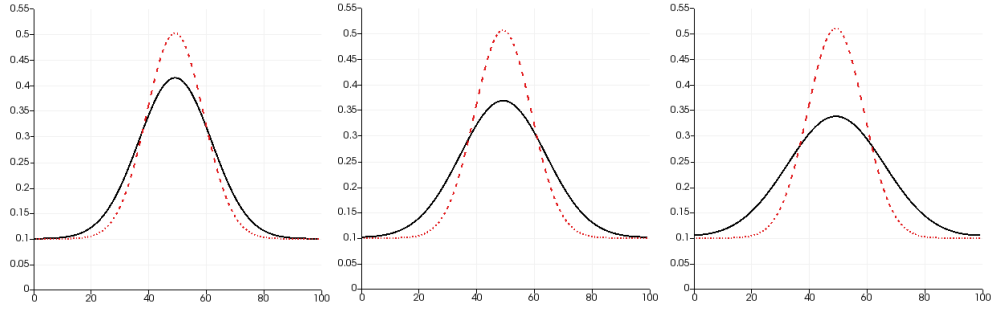


Figure 5.12: Discontinuous Galerkin approximation (advection equation) after 1, 2 and 3 full "circles"



Courant number) is given in figure 5.13. The superiority of the discontinuous Galerkin method increases with increasing time.

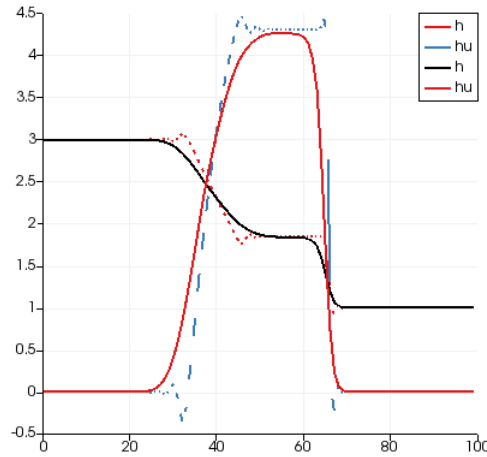
Figure 5.13: Comparison between finite volume method and discontinuous Galerkin method for the advection equation after 1, 2 and 3 full "circles" (red: discontinuous Galerkin, black: finite volumes)



5.4.2 Shallow Water Equations

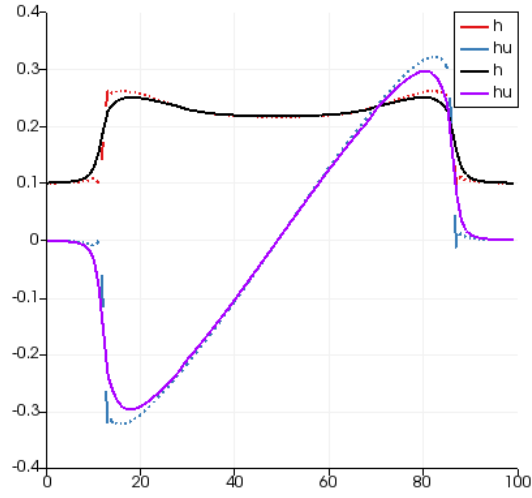
For the shallow water equations, in principle the same effects occur. Also it is clearly visible that discontinuous Galerkin methods are able to compute results closer to the analytic solution, especially at the location of the shock wave, as visualized in figure 5.14.

Figure 5.14: Comparison between finite volume method and discontinuous Galerkin method for the shallow water equations at $t=3$ (dotted lines: discontinuous Galerkin, continuous line: finite volumes)



For Gaussian hump starting conditions, the observed effects are mainly the same. Again, the dissipation in the finite volume method is too high and gets worse over time (see figure 5.15).

Figure 5.15: Comparison between finite volume method and discontinuous Galerkin method for SWE, gaussian hump, at $t=12.5$ (dotted lines: discontinuous Galerkin, continuous line: finite volumes)



5.5 Error estimation

The error is computed using the normalized p-norm for $p=2$.

$$error = \sqrt{\Delta x \left(\frac{\sum_{i=1}^I (u_i^{num} - u_i^{exc})^2}{\sum_{i=1}^I (u_i^{exc})^2} \right)} \quad (5.13)$$

where I is the number of intervals in the domain. The domain size is 100. For discontinuous Galerkin methods, the error computation includes the sum over the values of all nodes for both the analytic as well as the analytic solution.

For finite volumes, the expected result is linear convergence, at least down to machine accuracy [Lev04, p.143]. For discontinuous Galerkin solvers convergence is limited by the choice of integration method, as well as grid spacing [HW08, ch.4]. For an explicit Euler step, order of convergence is expected to be two.

5.5.1 Advection equation

Figure 5.16 plots the error against the number of intervals for the simple advection equation and the ideal curve for linear convergence (blue). The results show the expected behaviour. Since all values are stored in variables of type long double, machine accuracy is not a factor limiting the decrease of the error.

The absolute value of the error of the discontinuous Galerkin method (also computed with (5.13)) is smaller by a factor of around 10 than its finite volumes counterpart. Also it converges with a rate of two and thus shows a better convergence behaviour. The results are visualized in figure 5.17.

If instead of an explicit Euler step the midpoint method is used, the expected result has order of convergence 3. The visualization in figure 5.18 documents that the error for the used implementation shows this behaviour. Using the midpoint method slows the computation of results and error noticeably. This is caused by needing twice as much computations per time step. It also shows that the method is limited by the convergence behaviour of the used integration method.

5.5.2 Shallow water equations

For the shallow water equations, the expected orders of convergence are the same as for the advection equation. Error computing is now done by comparing the numerical approximation with the analytic solution at a predetermined time $t = 0.5$. The results are visualized in figures 5.19, 5.20 and 5.21. For the finite volume method, the error of

h behaves as expected, however, the error of hu doesn't show linear convergence, but decreases too slow. Since the error of hu dominates the total error because it has much higher absolute values than the error of h , the total error also shows this behaviour. The same occurs also for the discontinuous Galerkin solver. If only h is evaluated, the finite volume solver shows linear convergence and the discontinuous Galerkin solvers show convergence somewhat slower than the expected values of 2 or 3.

Figure 5.16: Diagram plotting error (black) ($p=2$ norm) and ideal curve for linear convergence (blue) and against number of intervals for a finite volume solver, CFL=0.4, advection equation. Logarithmic scale

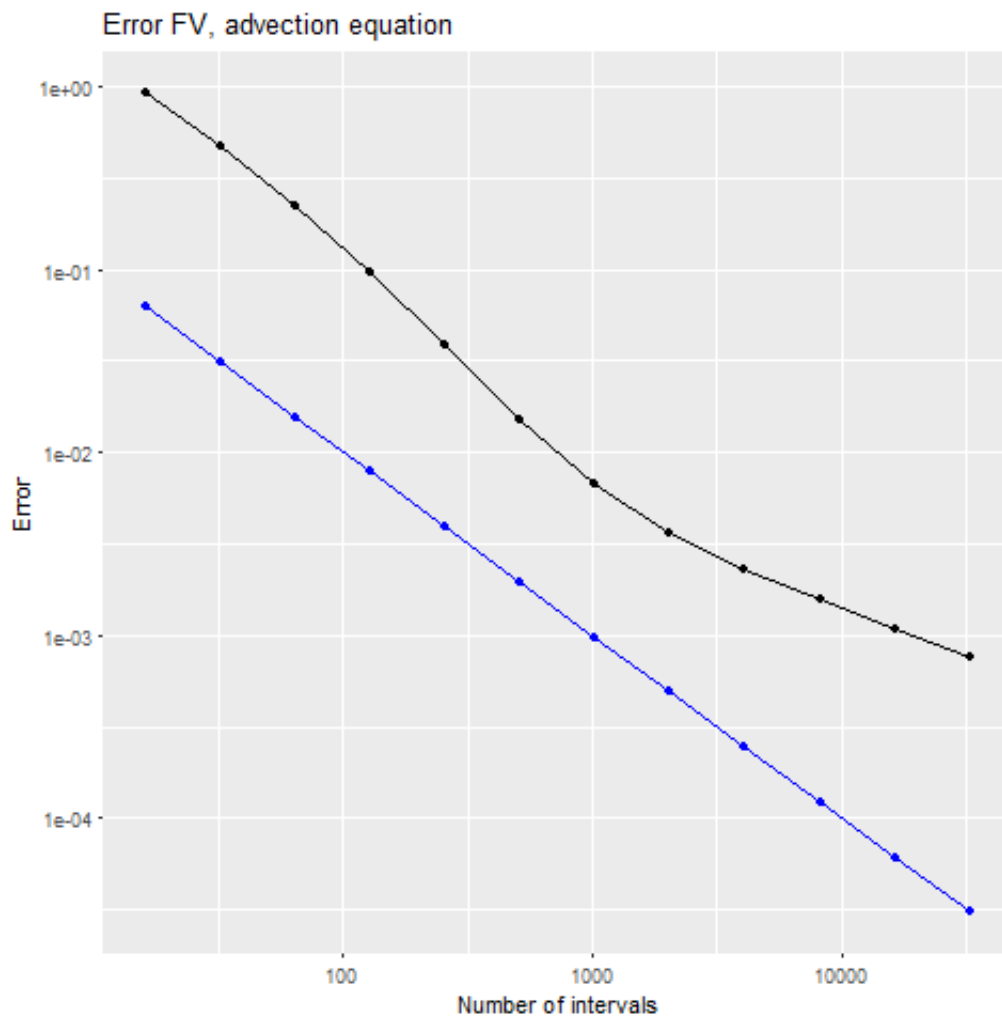


Figure 5.17: Diagram plotting error (black) (p-norm, $p=2$) and ideal curve for quadratic convergence (blue) and against number of intervals for a discontinuous Galerkin solver, CFL=0.04, advection equation. Logarithmic scale

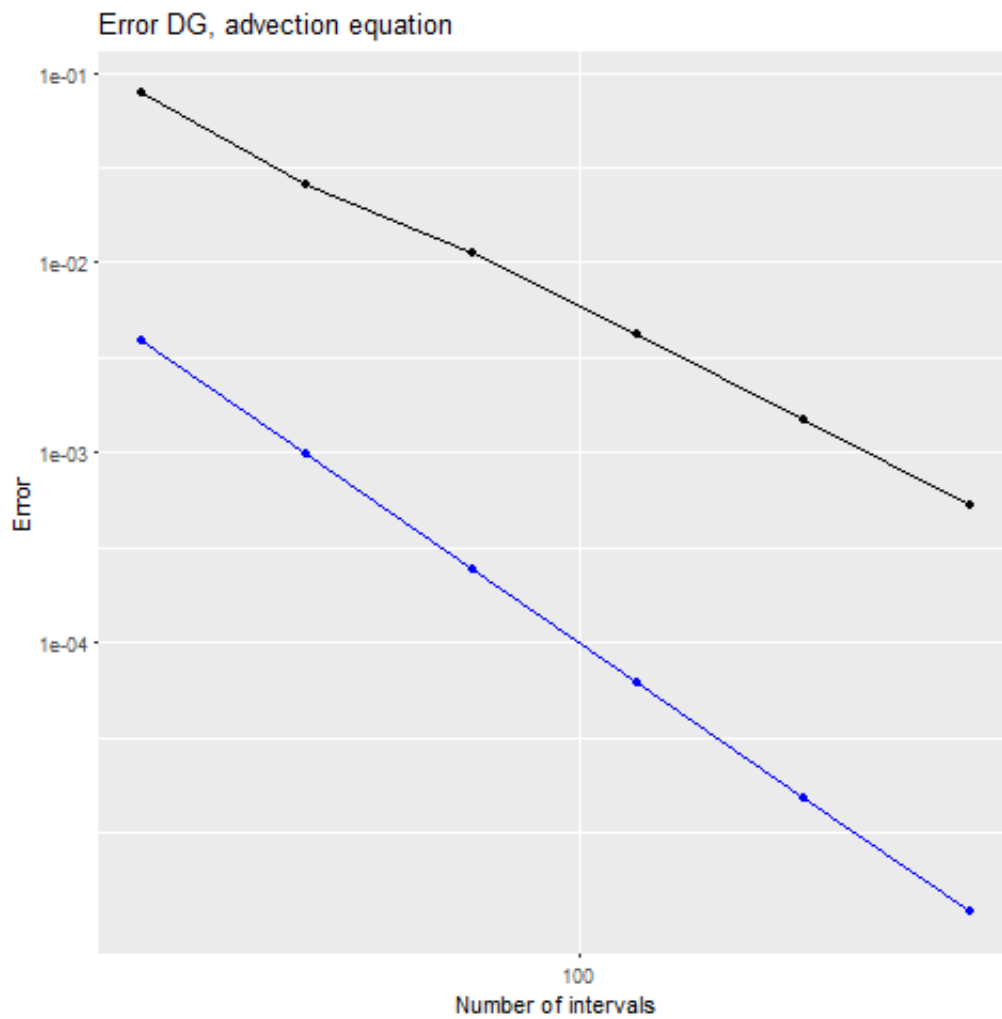


Figure 5.18: Diagram plotting error (black) (p-norm, $p=2$) and ideal curve for rate of convergence 3 (blue) against number of intervals for a discontinuous Galerkin solver, midpoint method, CFL=0.04, advection equation. Logarithmic scale

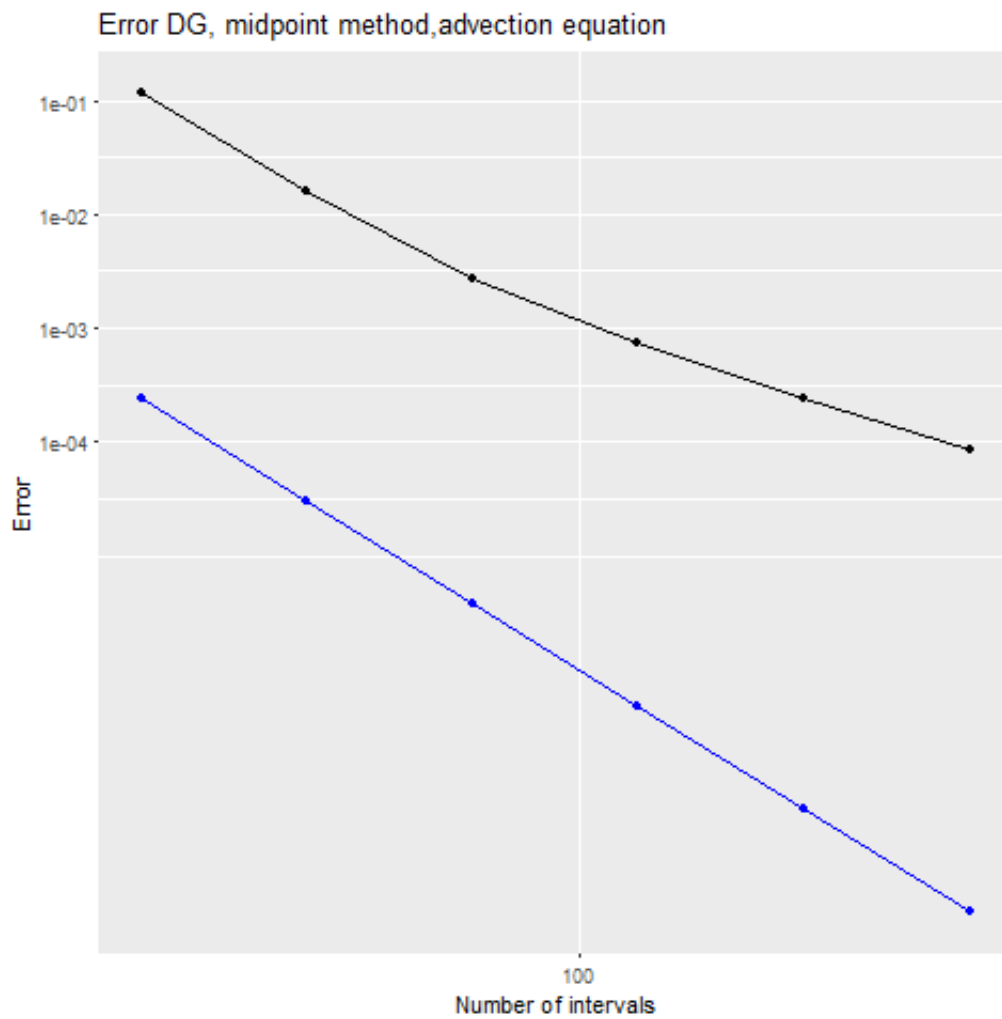


Figure 5.19: Diagram plotting cumulated error (black), error of h (red), error of hu (green) (p-norm, $p=2$) and ideal curve for linear convergence (blue) against number of intervals for a finite volume solver, CFL=0.04, shallow water equations. Logarithmic scale

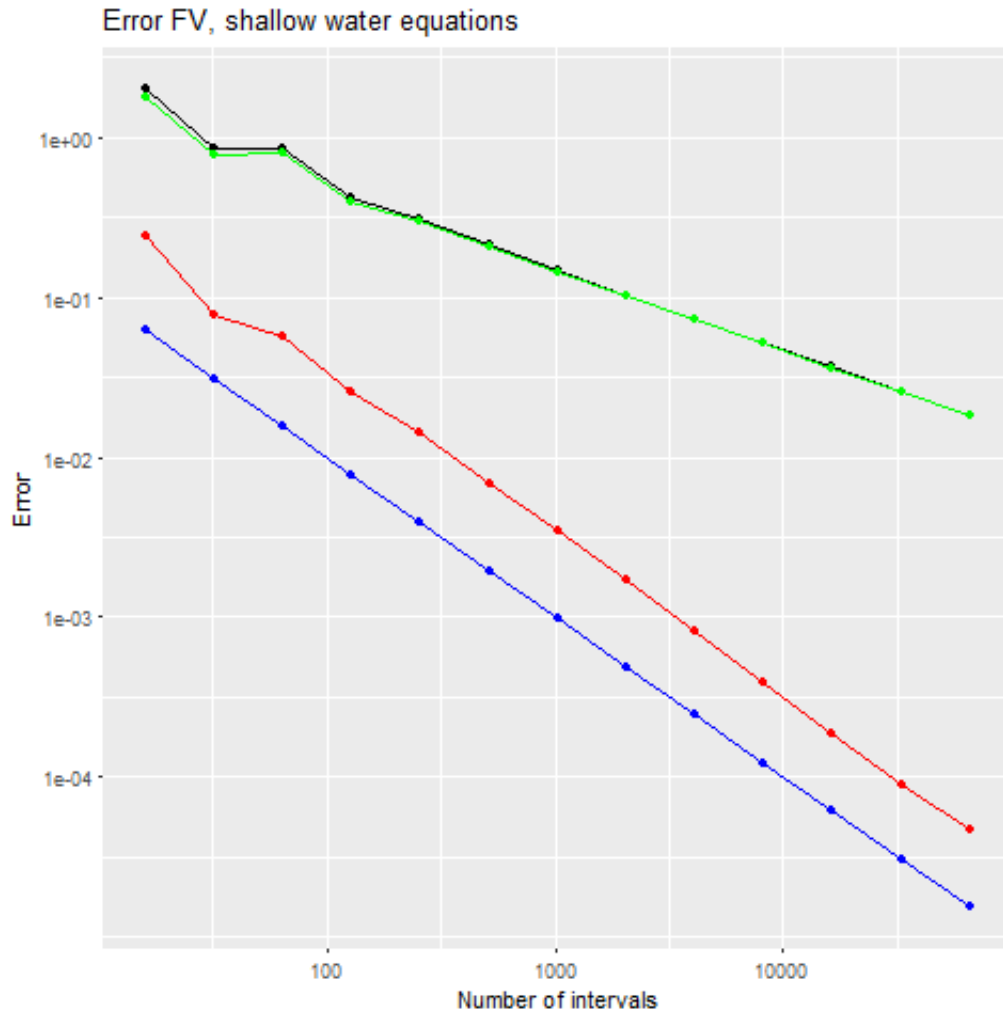


Figure 5.20: Diagram plotting cumulated error (black), error of h (red), error of hu (green)(p-norm, $p=2$) and ideal curve for quadratic convergence (blue) against number of intervals for a discontinuous Galerkin solver, CFL=0.04, shallow water equations. Logarithmic scale

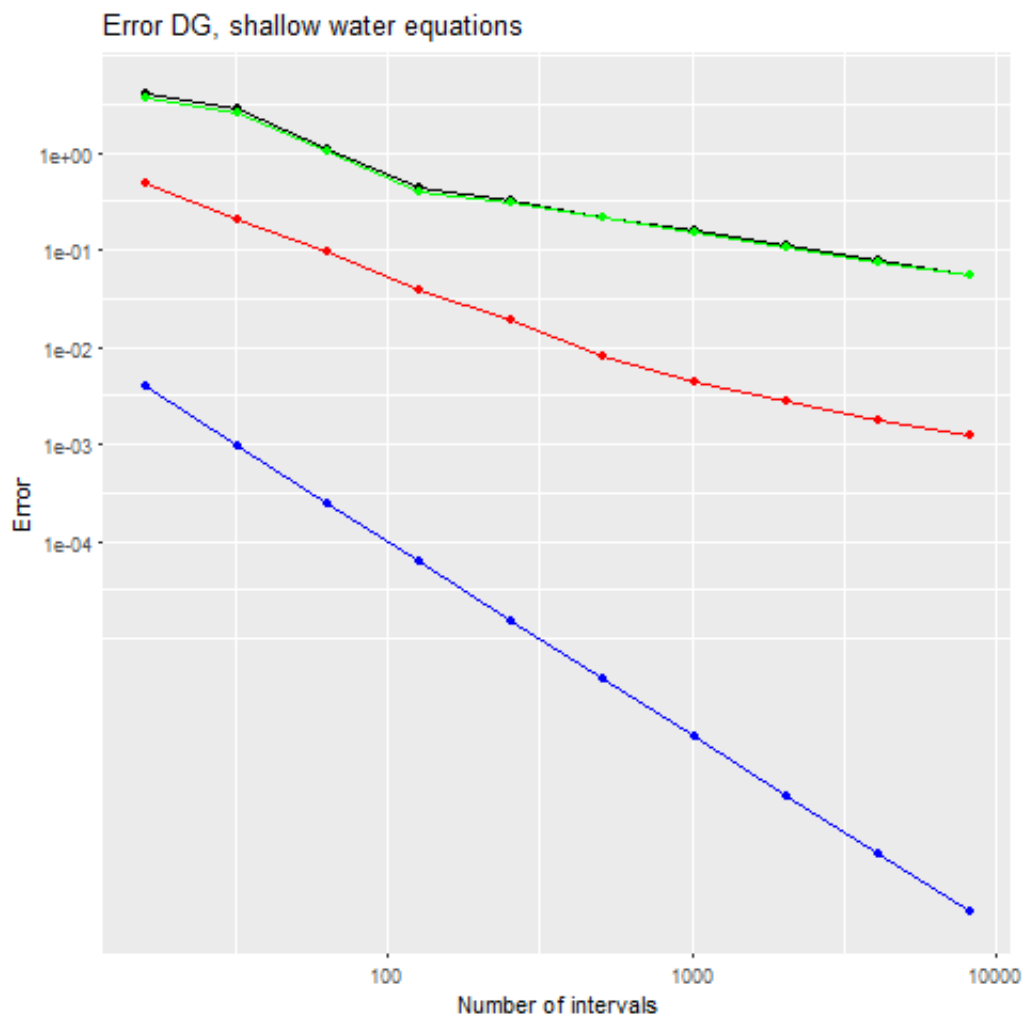
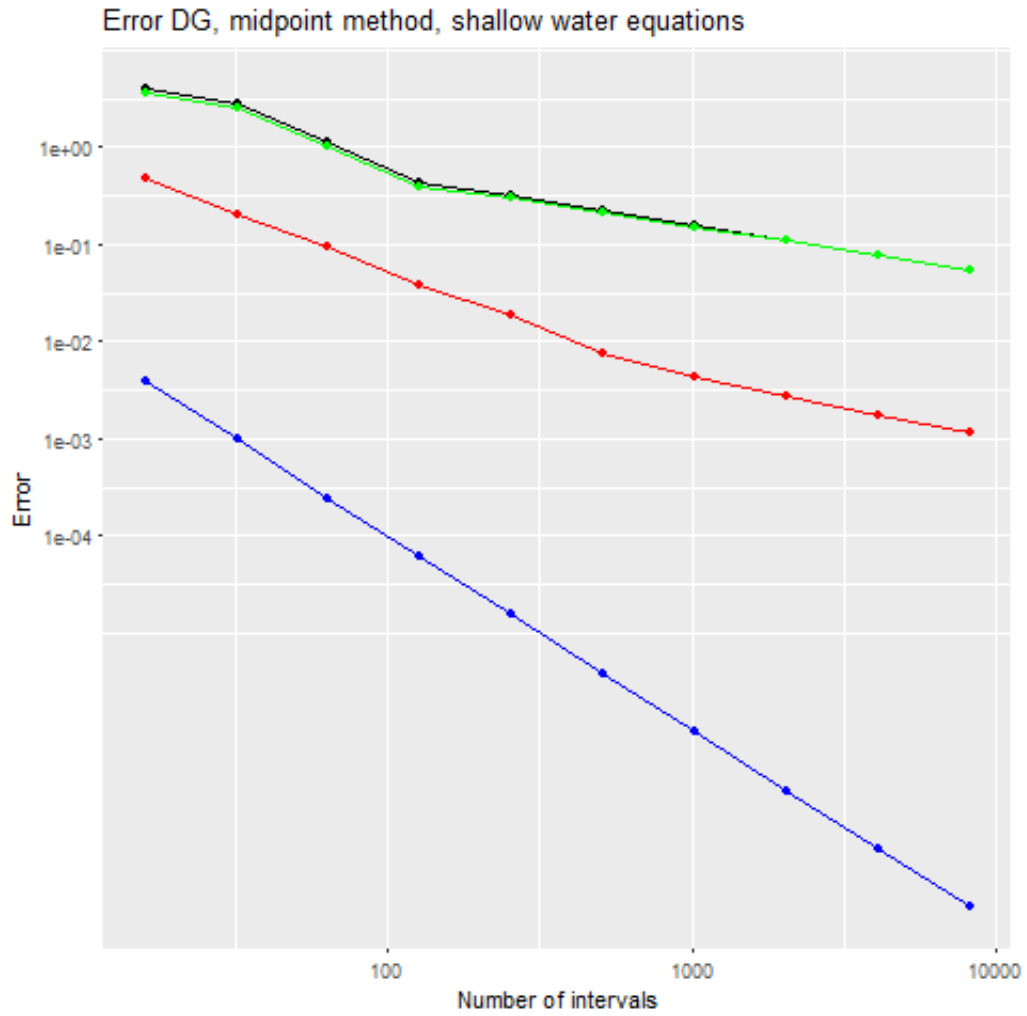


Figure 5.21: Diagram plotting cumulated error (black), error of h (red), error of hu (green)(p-norm, $p=2$) and ideal curve for rate of convergence 3 (blue) against number of intervals for a discontinuous Galerkin solver, midpoint method, CFL=0.04, advection equation. Logarithmic scale



6 Conclusion

While the tested finite volume approach solves problem with continuous initial conditions reasonably well, at least when a local Lax-Friedrichs flux is used and the simulation does not run for too long, and it might seem like the usage of the discontinuous Galerkin method is unnecessary for those easier cases, the results differ vastly when a dam-break problem has to be solved. The comparison clearly shows that a discontinuous Galerkin solver can handle discontinuities a lot better and also does not have the problem of too much dissipation. Even the numerical solution of the advection equation, which is otherwise quite close to the analytic solution, shows too much dissipation when solved with finite volumes. So even if a problem is continuous and otherwise very simple, using a discontinuous Galerkin solver can be beneficial when later times shall be evaluated. Since discontinuous Galerkin methods were designed especially for solving hyperbolic PDEs and conservation laws, they are the preferable choice of numerical method for most of these equation systems. These methods also have the advantage that if two different systems of PDEs shall be solved and the used basis and test functions stay the same, then all used matrices (stiffness, mass and the ones applied to right and left fluxes) stay the same and can be reused without computing them again. This means that those pre-computed matrices can be used as a framework for solving several different equation systems.

The theory and methods presented in this thesis can be adapted to more-dimensional problems or other systems of hyperbolic PDEs. Analyzing the error and its convergence made it clear that for a higher order of accuracy for a discontinuous Galerkin method it would be necessary to use higher order integration methods such as standard Runge-Kutta.

Appendix

1 Detailed derivation of matrices for discontinuous Galerkin method

$$\forall i \in 1 \dots N$$

$$\sum_j \int_{I_i} \varphi_i ((\varphi_j u_j)_t + a(\varphi_j u_j)_x) dx = 0$$

$$\sum_j \int_{I_i} \varphi_i (\varphi_j (u_j)_t + a(\varphi_j)_x u_j) dx = 0$$

$$\sum_j \int_{I_i} \varphi_i \varphi_j (u_j)_t + a \varphi_i (\varphi_j)_x u_j dx = 0$$

$$\sum_j \int_{I_i} \varphi_i \varphi_j (u_j)_t dx + a \int_{I_i} \varphi_i (\varphi_j)_x u_j dx = 0$$

$$\sum_j \int_{I_i} \varphi_i \varphi_j (u_j)_t dx - a \int_{I_i} \varphi_j u_j (\varphi_i)_x dx + \int_{\delta I_i} \varphi_i \varphi_j u_j \vec{n} dx = 0$$

$$\sum_j \int_{I_i} \varphi_i \varphi_j (u_j)_t dx - a \int_{I_i} \varphi_j u_j (\varphi_i)_x dx + (\varphi_i \varphi_j a u_j)|_{x_l} - (\varphi_i \varphi_j a u_j)|_{x_r} = 0$$

$$\sum_j \int_{I_i} \varphi_i \varphi_j (u_j)_t dx - a \int_{I_i} \varphi_j u_j (\varphi_i)_x dx + (\varphi_i \varphi_j)|_{x_l} ((au)^*)_l - (\varphi_i \varphi_j)|_{x_r} ((au)^*)_r = 0$$

2 Overview over computed errors

2.1 Advection equation - finite volumes

No. of intervals	16	32	64	128	256
Error	0,930347	0,473809	0,224143	0,0950829	0,0381764
No. of intervals	512	1024	2048	4096	8192
Error	0,0152314	0,00669867	0,00358239	0,00227265	0,00155586
No. of intervals	16384	32768			
Error	0,00109038	0,000757024			

Table 1: Computed errors for Courant number = 0.4, advection equation, finite volumes method

2.2 Advection equation - discontinuous Galerkin

No. of intervals	16	32	64	128	256
Error	0,07879	0,0257228	0,0112365	0,00417732	0,00149142
No. of intervals	512				
Error	0,000527922				

Table 2: Computed errors for Courant number = 0.04, advection equation, discontinuous Galerkin method

2.3 Advection equation - discontinuous Galerkin and midpoint method

No. of intervals	16	32	64	128	256
Error	0,117877	0,0160371	0,00269389	0,000735596	0,00024506
No. of intervals	512				
Error	0,0000854233				

Table 3: Computed errors for Courant number = 0.04, advection equation, discontinuous Galerkin method, midpoint method

2.4 Shallow water equations - finite volumes

No. of intervals	16	32	64	128	256
Error	2,03685	0,860466	0,850186	0,419891	0,311018
Error (h)	0,244086	0,0765507	0,0564617	0,0255438	0,0141828
Error (hu)	1,79277	0,783916	0,793724	0,394348	0,296835
No. of intervals	512	1024	2048	4096	8192
Error	0,216973	0,148812	0,103554	0,0727068	0,0518031
Error (h)	0,00684068	0,00344795	0,0016949	0,000821448	0,000394643
Error (hu)	0,210133	0,145364	0,101859	0,0718854	0,0514085
No. of intervals	16384	32768	65536		
Error	0,0366241	0,0258926	0,0183371		
Error (h)	0,00018838	0,0000897923	0,0000463219		
Error (hu)	0,0364358	0,0258028	0,0182908		

Table 4: Computed errors for Courant number = 0.4, SWE, finite volumes method

2.5 Shallow water equations - discontinuous Galerkin

No. of intervals	16	32	64	128	256
Error	4,13947	2,79617	1,12014	0,444392	0,331104
Error (h)	0,490054	0,201237	0,0939928	0,0384971	0,0192858
Error (hu)	3,64942	2,59493	1,02615	0,405895	0,311818
No. of intervals	512	1024	2048	4096	8192
Error	0,220701	0,156397	0,110509	0,0778694	0,0555034
Error (h)	0,00790505	0,00447998	0,00277195	0,00178803	0,00121357
Error (hu)	0,212796	0,151917	0,107737	0,0760813	0,0542899

Table 5: Computed errors for Courant number = 0.4, SWE, discontinuous Galerkin method

2.6 Shallow water equations - discontinuous Galerkin and midpoint method

No. of intervals	16	32	64	128	256
Error	4,03825	2,75989	1,10133	0,424437	0,32244
Error (h)	0,484444	0,202624	0,0927935	0,0376708	0,0189471
Error (hu)	3,55381	2,55727	1,00854	0,386766	0,303493
No. of intervals	512	1024	2048	4096	8192
Error	0,217268	0,154077	0,109629	0,0773891	0,0552412
Error (h)	0,00768793	0,00427299	0,00267747	0,00172422	0,00117246
Error (hu)	0,20958	0,149804	0,106951	0,0756649	0,0540687

Table 6: Computed errors for Courant number = 0.4, SWE, discontinuous Galerkin method, midpoint method

List of Figures

3.1	Comparison of the advantages and disadvantages of different methods (FDM = finite differences, FVM = finite volumes, FEM = finite elements, DG-FEM = discontinuous Galerkin) to solve hyperbolic PDEs, source [HW08, p.7]	19
4.1	Two shocks - Paraview visualization of a numerical approximation to a problem with $u_l = 2$, $u_r = -2$ and $h_0 = 3$ at time $t \approx 2.65$ for a computational domain of size 100, horizontal axis x position, vertical axis h and u	23
4.2	Two rarefaction waves - Paraview visualization of a numerical approximation to a problem with $u_l = -2$, $u_r = 2$ and $h_0 = 3$ at time $t \approx 2.65$ for a computational domain of size 100, horizontal axis x position, vertical axis h and u	24
4.3	1 rarefaction, 1 shock - Paraview visualization of the exact solution to a problem with $u_l = u_r = 0$, $h_l = 3$ and $h_r = 1$ at time $t \approx 2.65$ for a computational domain of size 100, horizontal axis x position, vertical axis h and hu	25
5.1	Paraview visualization of the initial conditions following a Gaussian distribution for a computational domain of size 100	30
5.2	Paraview visualization of the initial conditions of the used dam-break problem for a computational domain of size 100	31
5.3	Evolution of the solution to the dam break problem using an unstable flux, $t=1.4$, $t=2.7$ and $t=5.2$	35
5.4	Evolution of the solution of the dam break problem using Lax-Friedrichs flux, $t_1=1.4$, $t_2=2.7$, $t_3=5.2$	35
5.5	Evolution of the solution of the gaussian water hump using Lax-Friedrichs flux, $t_1=5.4$, $t_2=10.1$, $t_3=15.3$	36
5.6	Evolution of the solution of the dam break problem using a local Lax-Friedrichs flux, $t_1=1.4$, $t_2=2.7$, $t_3=5.2$	36
5.7	Evolution of the solution of the gaussian water hump using a local Lax-Friedrichs flux, $t_1=5.4$, $t_2=10.1$, $t_3=15.3$	37
5.8	DG approximation (advection equation) after 1, 2 and 3 full "circles" . .	39

5.9	DG approximation (SWE, dam break) $t_1=1.4$, $t_2=2.7$, $t_3=5.2$	40
5.10	DG approximation (SWE, gaussian) $t_1=5.4$, $t_2=10.1$, $t_3=15.3$	40
5.11	Finite volume approximation (advection equation) after 1, 2 and 3 full "circles"	41
5.12	Discontinuous Galerkin approximation (advection equation) after 1, 2 and 3 full "circles"	41
5.13	Comparison between finite volume method and discontinuous Galerkin method for the advection equation after 1, 2 and 3 full "circles" (red: discontinuous Galerkin, black: finite volumes)	42
5.14	Comparison between finite volume method and discontinuous Galerkin method for the shallow water equations at $t=3$ (dotted lines: discontinuous Galerkin, continuous line: finite volumes)	42
5.15	Comparison between finite volume method and discontinuous Galerkin method for SWE, gaussian hump, at $t=12.5$ (dotted lines: discontinuous Galerkin, continuous line: finite volumes)	43
5.16	Diagram plotting error (black) ($p=2$ norm) and ideal curve for linear convergence (blue) and against number of intervals for a finite volume solver, CFL=0.4, advection equation. Logarithmic scale	46
5.17	Diagram plotting error (black) (p -norm, $p=2$) and ideal curve for quadratic convergence (blue) and against number of intervals for a discontinuous Galerkin solver, CFL=0.04, advection equation. Logarithmic scale	47
5.18	Diagram plotting error (black) (p -norm, $p=2$) and ideal curve for rate of convergence 3 (blue) against number of intervals for a discontinuous Galerkin solver, midpoint method, CFL=0.04, advection equation. Logarithmic scale	48
5.19	Diagram plotting cumulated error (black), error of h (red), error of h_u (green) (p -norm, $p=2$) and ideal curve for linear convergence (blue) against number of intervals for a finite volume solver, CFL=0.04, shallow water equations. Logarithmic scale	49
5.20	Diagram plotting cumulated error (black), error of h (red), error of h_u (green) (p -norm, $p=2$) and ideal curve for quadratic convergence (blue) against number of intervals for a discontinuous Galerkin solver, CFL=0.04, shallow water equations. Logarithmic scale	50
5.21	Diagram plotting cumulated error (black), error of h (red), error of h_u (green) (p -norm, $p=2$) and ideal curve for rate of convergence 3 (blue) against number of intervals for a discontinuous Galerkin solver, midpoint method, CFL=0.04, advection equation. Logarithmic scale	51

List of Tables

1	Computed errors for Courant number = 0.4, advection equation, finite volumes method	B
2	Computed errors for Courant number = 0.04, advection equation, discontinuous Galerkin method	B
3	Computed errors for Courant number = 0.04, advection equation, discontinuous Galerkin method, midpoint method	B
4	Computed errors for Courant number = 0.4, SWE, finite volumes method	C
5	Computed errors for Courant number = 0.4, SWE, discontinuous Galerkin method	C
6	Computed errors for Courant number = 0.4, SWE, discontinuous Galerkin method, midpoint method	D

Bibliography

- [al.16] O. D. et al. *SWASHES: a compilation of Shallow Water Analytic Solutions for Hydraulic and Environmental Studies*. 2016.
- [Bre04] M. Breuss. "The correct use of the Lax-Friedrichs method." In: *ESAIM: Mathematical Modelling and Numerical Analysis* 38.3 (2004).
- [BZBP13] H.-J. Bungartz, S. Zimmer, M. Buchholz, and D. Pflüger. *Modellbildung und Simulation - Eine anwendungsorientierte Einführung*. eXamen.press. Springer Spektrum, 2013. ISBN: 978-3-642-37655-9.
- [HW08] J. S. Hesthaven and T. Warburton. *Nodal Discontinuous Galerkin Methods - Algorithms, Analysis, and Applications*. Texts in Applied Mathematics. Springer, 2008. ISBN: 978-0-387-72065-4.
- [Lev04] R. J. Leveque. *Finite Volume Methods for Hyperbolic Problems*. Cambridge Texts in Applied Mathematics. Cambridge University Press, 2004. ISBN: 0-521-81087-6.
- [Ret] S. Rettenberger. *SWE1D github page*.
- [Sto57] J. J. Stoker. *Water Waves - The Mathematical Theory with Applications*. Pure and Applied Mathematics - A Series of Texts and Monographs. Interscience Publishers, Inc., New York, 1957. ISBN: 978-0471570349.
- [Stu13] U. Stuttgart. *Skript Partielle Differentialgleichungen II*. 2013.